Heritage Science

RESEARCH

Open Access

Infrared spectroscopy reveals the reactivity of fatty acids on copper surfaces and its implications for cultural heritage objects

Stamatis C. Boyatzis[1*], Leonidas Fragkos-Livanios[1,2], Maria Giannoulaki[1] and Anna Filopoulou[1]

Abstract

The reactivities of various fatty monoacids and diacids on copper metal-containing surfaces were investigated through reflection–absorption infrared spectroscopy. The formation of copper carboxylates is detected on pure copper surfaces, while copper and zinc carboxylates are simultaneously formed on brass surfaces. Following the decrease of acid carbonyl and the formation of carboxylate infrared bands, it is shown that fatty monoacids C8 and C10 react with clean/polished copper and its zinc alloy within 2–4 h, while those with chains > C12 react within days. At the end of the processes, only the corresponding metal carboxylates are detected in all cases. An explanation for the above is offered on a molecular mobility and acidity basis, where the lower monoacids (liquids in room temperature), also having lower pK_a values, favor higher reaction rates. Furthermore, it is argued that longer-chain fatty monoacids, when deposited from their solutions, allow for favorable orientation resulting in self-assembled monolayer-type molecular packing on the copper surface, which may additionally rationalize the slower reaction. Interestingly, fatty diacids do not form any carboxylate products under the same conditions, as it is argued that their molecules may efficiently pack as self-assembled multilayers on copper and ultimately protect it. The possible implications of the fatty monoacid and diacid behavior on the archaeological organic residues level and regarding the stability of copper alloys are discussed.

Keywords Fatty acids, Reactivity, Copper, Brass, Carboxylates

Introduction

Organic residues in archaeological copper alloy containers for cosmetics, burning oils used in rituals, and eventually, nutritional residues, may contain fatty substances, which can easily undergo hydrolytic degradation [1–4], mainly caused by environmental humidity, in the presence of acids (such as atmospheric carbon dioxide), or bases (such as carbonates, hydroxy salts, etc.) [5–9]. Furthermore, oxidation pathways in unsaturated oils can produce oxygen-containing products including dicarboxylic acids [10–13]. The main products of this ubiquitous process are free fatty acids, which may stay on the metal surface for as long as their reactivity towards basic substances (i.e., metal oxides, hydroxides, carbonates, etc.) and metals (such as iron, and copper) permits.

Strangely, relatively few studies have been conducted for investigating copper salts in the context of organic residues in copper alloy vessels [14–18] or other copper surfaces [19–21]. Specifically, little attention was given to the sources and formation pathways of these carboxylates. On the other hand, metal soaps, such as those of zinc, lead, and copper, have been detected in the course of investigations in art paintings, where they have been considered as the saponification products of oil binders with copper-containing pigments [22–27].

*Correspondence:
Stamatis C. Boyatzis
sboyatzis@uniwa.gr
[1] Department of Conservation of Antiquities and Works of Art, University of West Attica, 12243 Egaleo, Greece
[2] Hellenic Army Academy, 16673 Vari, Greece

The reactivity of copper metal towards carboxylic acids is of course not new; in the notable example of acetic acid attacking copper metal to form copper acetates of various structures, the historical pigment verdigris is formed [28–30], the structure and alterations of which have lately received renewed attention [31, 32]. This reaction is enabled in an aqueous environment, which allows the dissociation of acetic acid and oxygen forming an energetically favored redox pair with copper. However, questions regarding the reactivity of fatty acids (FA) with copper metal towards forming the corresponding carboxylates have been left in the dark, with only a few exceptions. In 1954, a Nature paper was published briefly reporting the interaction of fatty acid monolayers in the form of Langmuir–Blodgett (LB) films with copper reporting that no reaction may occur in an inert atmosphere, as oxygen is needed in the redox cycle [33]. Another publication in 1983 reported on the heterogeneous reaction of copper surfaces with stearic acid resulting in copper carboxylate with an infrared maximum of its symmetric stretch at 1590 cm^{-1} [34]. In the fields of art and culture in particular, few publications acknowledge the saponification of fats [19, 35] and waxes [36, 37] on copper surfaces. Later (2006), a systematic study regarding the degradation of oil- and wax-painted copper surfaces was reported [21], while more recently, efflorescence on oil-covered copper alloy surfaces attributed to copper soaps was visually detected and characterized by FTIR [38]. In all the above, however, no further details have been offered on the fatty acid reaction pathways on the surface of copper metal.

On the other hand, iron has been well-investigated in a similar context. Studies conducted on the surface of iron metal and iron oxides have shown that long-chain fatty monoacids (FMA) such as stearic, oleic, and linoleic are similarly reactive towards these surfaces; this was shown to be favored by monomolecular chemisorption of FMA mainly through their carboxyl functionality. This phenomenon induces a significant effect on the tribological parameters of steel metallic parts; the lubrication industry was taken advantage of this phenomenon towards formulations for reducing friction in machinery [39].

In the context of understanding the behavior of long alkyl chain molecules bearing polar functionalities, considerable research has been done on the ability of fatty acids to form self-assembled monolayers (SAMs) on typical 'noble' metals, such as gold, silver, and copper [39–42]. FMA alkyl chains higher than C10 favor the formation of SAMs, as the carboxylic groups anchor on thin oxide films formed on the metal surfaces. It is interesting to point out that SAMs have been shown to offer metal protection by forming anticorrosion films on such metals [43].

In light of the above, the following questions arise: (a) could copper carboxylates detected in archaeological organic residues, originate through the direct interaction of free FA with copper metal (b) can the carboxylate formation be directly demonstrated through spectroscopy? (c) How fast is this interaction occurring for various FMA and fatty diacids (FdiA)?

In a previous study [14], the presence of a wide range of FA and their metal soaps on the surface of metal vessels through screening of organic residues inside copper alloy containers from the early Christian era in Egypt (3–4th c. AD) has been shown employing infrared spectroscopy, while a wide array of FMA and FdiA was detected through gas chromatography-mass spectrometry (GC–MS). The variety of both types of identified acids, as well as the amounts of the detected metal fatty carboxylates, is impressive. Besides, an attempted infrared spectroscopic study of the above organic residues through solvent extraction and subsequent deposition on mirror-like copper-zinc alloy surface showed the formation of carboxylates within a matter of a few days or even hours; this is shown in Fig. 1. The collection of these experimental data inspired this study.

Copper soaps have been detected on the surface of beeswax-covered metal objects, and explanations were offered to rationalize this as the result of the reaction between the copper metal and free fatty acids formed after wax degradation [36, 37]. A proof of concept has been recently offered, illustrating the electrolytic formation of copper palmitate on the surface of copper coupon serving as the anode [44]; evidence for the formation of this specific soap was offered through FTIR and XRD.

Infrared spectroscopy has been highly successful in investigating metal soaps and distinguishing them from their fatty acid precursors [45–47]. The most important infrared feature of carboxylates is the symmetric and antisymmetric stretching vibrations of the carboxylate ion, generally occurring at 1600–1500 and 1420–1380 cm^{-1}. The actual maxima primarily depend on the metal cations and the type of coordination, while no significant dependence of carboxylate maxima on the fatty alkyl chain lengths has been observed [11, 13, 47–49].

An interesting vibrational feature associated with the symmetry of the metal-carboxylate coordination is the difference between the antisymmetric (ν_{as}) and symmetric (ν_s) bands (often called the 'delta', Δ), first introduced by Deacon and Phillips [50]; the higher the coordination symmetry, the lower the distance between the antisymmetric and symmetric maxima [51, 52]. Unidentate coordination assumes the highest Δ values, bridging geometries its lowest, while chelates and ionic

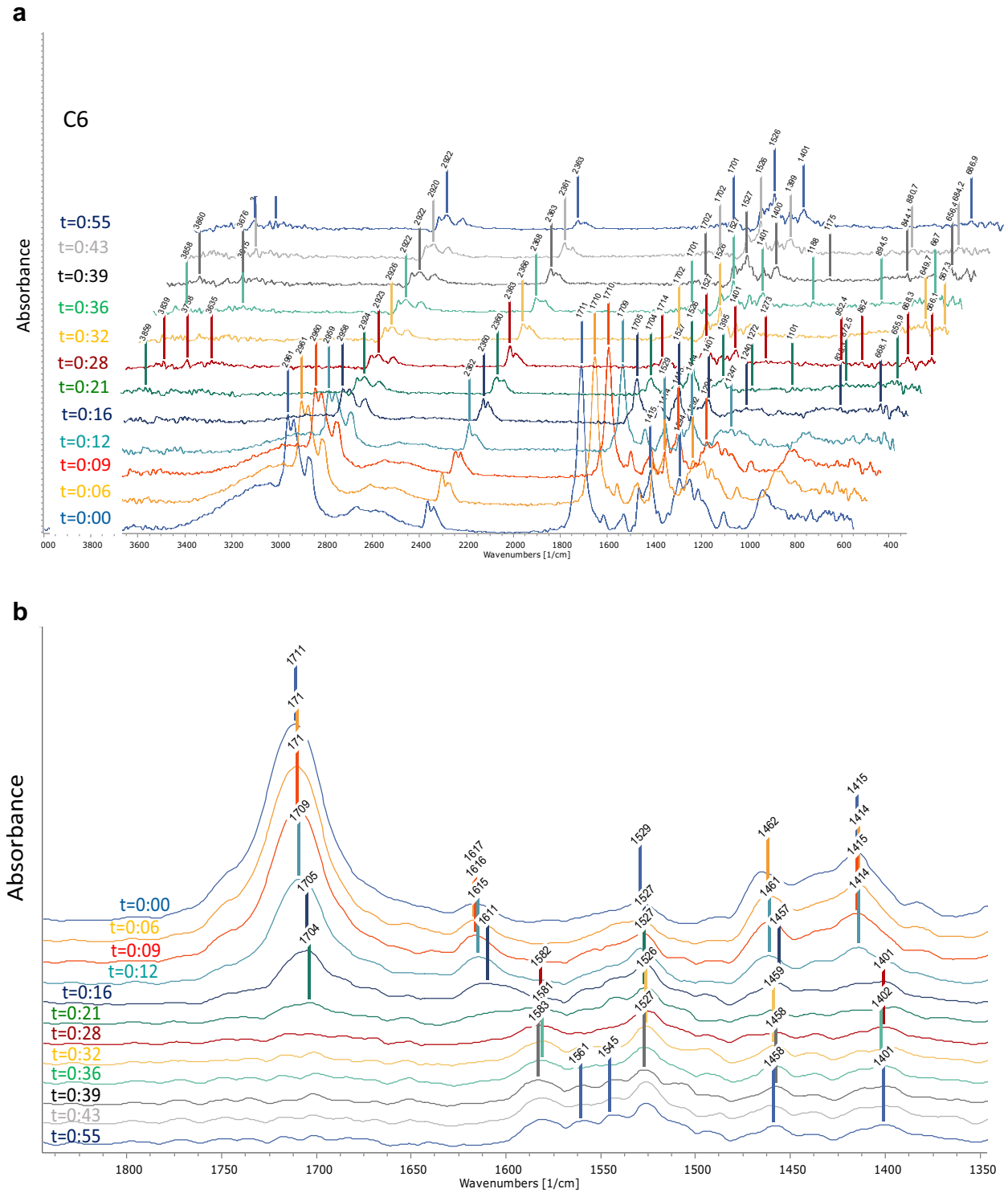

Fig. 1 Consecutive spectra of caproic acid (C6) after deposition on copper-zinc alloy surface **a** full spectra; **b** zooming in the region 1800–1350 cm^{-1} from the same spectra. Ambient temperature was recorded at 23 °C and RH at 37%; time is given in hours:minutes

structures (or salts) show intermediate values [47, 52, 53]. Besides, copper forms binuclear coordination complexes [54, 55] with ν_{as} approx. 1580–1587 cm^{-1} and the ν_s at 1415–1422 cm^{-1} with a $\Delta v \sim 165$ cm^{-1}, where a bidentate chelating geometry is obeyed [13, 39, 51].

Possibly, the most studied metal carboxylates are those of zinc and lead. The former are of interest to this present study, as the interaction of fatty acids on copper-zinc alloy (brass) surfaces is reasonably expected to involve zinc as well. The carboxylates have been found to have a variety of structures ranging from polymer-like 2D coordination structures with v_{as} antisymmetric maxima at 1535–1545 and 1525–1530 cm^{-1}. A tetranuclear complex with a maximum of 1590 cm^{-1}, as well as linear coordination polymer-like structures with maxima at 1630 and 1544 cm^{-1}, were also reported [24, 26, 45, 48, 56].

Relatively fewer data are available for copper carboxylates; crystal structure investigations have shown that the d-spacings of copper stearate are relatively higher than those of the corresponding zinc soap [46, 57], which correspond to higher distances between carboxylic moieties and affect their vibrational frequencies. Specifically, the antisymmetric infrared maxima reported for copper carboxylates to be at higher values (1585 cm^{-1}) than those of the zinc carboxylates with an additional one at 1508 cm^{-1}, while the symmetric band is found at 1415 cm^{-1} [47, 54] giving a Δ value of 170 cm^{-1}. Additionally, copper carboxylate infrared spectra have been reported to assume multinuclear coordination geometries [44, 46, 47], although clear data have been shown for the binuclear complexes, where two Cu(II) ions are bridged through four carboxylate units [54, 55]. These geometries are established on the basis of multiple carboxylate maxima (or 'multiplets') as shown below.

Among the typical C-H vibrations in the infrared spectra of the above types of molecules are the CH_2 and CH_3 stretching vibrations; especially the antisymmetric stretch in FA appears at 2940–2920 cm^{-1} heavily depending on the alkyl chain length (upshifted in shorter chains), while in the corresponding soaps, it is generally downshifted below 2920 cm^{-1} [13], which can serve as a diagnostic feature. Besides, the methyl wagging and twisting progressions (1400–1200 cm^{-1}), as well as their rocking vibrations (740–720 cm^{-1}), offer weak but significant features also depending on the chain length [13, 47]. These are useful for investigating the inter-chain interactions, which depend on the molecular alignment, most efficient in long alkyl chains.

A versatile, yet powerful method to investigate the formation of metal soaps on metal surfaces is reflection spectroscopy often termed *reflection–absorption infrared spectroscopy* (RAIRS) in the case of thin organic films, or *transflection* in the case of thicker films. This technique is capable of investigating layered organic materials, ideally, film-forming, along the z-axis perpendicular to the metal surface [58–61]. It can therefore be used to record fatty acids in the form of deposited layers on a reflecting surface of copper metal and its alloys and their transformation into their metal salts [59, 61–65]. In this paper, we demonstrate our results on the reactivities of various fatty monoacids and diacids on copper metal-containing surfaces; the reactivities among various acids with different alkyl chain lengths are compared.

Materials and methods

Materials

Fatty acid standards were purchased from Sigma-Aldrich: octanoic, or caprylic acid ($CH_3(CH_2)_6COOH$ or C8:0, ≥ 99%), decanoic, or capric acid ($CH_3(CH_2)_8COOH$ or C10:0, > 98.0%), dodecanoic, or lauric acid ($CH_3(CH_2)_{10}COOH$ or C12:0, ≥ 99%), tetradecanoic, or myristic acid ($CH_3(CH_2)_{12}COOH$ or C14:0, ≥ 99%), hexadecanoic or palmitic ($CH_3(CH_2)_{14}COOH$ or C16:0, ≥ 99%), octadecanoic, or stearic acid ($CH_3(CH_2)_{16}COOH$ or C18:0, ≥ 98.5%), octanedioc, or suberic acid ($C_6H_{12}(COOH)_2$ or C8di, 98%) and nonanedioic, or azelaic acid ($C_7H_{14}(COOH)_2$ or C9di, 98%).

Additional reagents and solvents were acquired as follows: sodium hydroxide (Sigma-Aldrich > 98%), water (Honeywell, HPLC grade), copper sulfate (anhydrous, Sigma-Aldrich, ≥ 98%), ethanol (Merck, 99.5%), chloroform (Sigma-Aldrich, anhydrous, ≥ 99%, acetone (Honeywell (≥ 99.5%).

Synthesis of copper FA carboxylate authentics

Copper salts of fatty acids C8:0, C10:0, C12:0, C14:0, C16:0, C18:0, C8di, and C9di were synthesized in two steps, analogously to a previously published procedure [13]. In the first step, 0.1 mmol of the corresponding acids were neutralized by adding 1 mL of 0.1 M sodium hydroxide aqueous solution (corresponding to 1 equivalent of the base) under stirring; for the diacid (C8di and C9di) sodium salts, two equivalents of the base were added. A white precipitate (the sodium soap) was formed for C12:0, C14:0, and C18:0. In the second step, 1 mL of anhydrous copper sulfate 0.1 M (1 equivalent) was added per 2 equivalents of the fatty monocarboxylic acids and per 1 equivalent of the two fatty diacids. In all cases, an intensely blue precipitate was formed. In the cases of C12:0, C14:0, C16 and C18:0, C8di, and C9di, the copper salt formation was assisted by sonicating the mixture for 15 min. The infrared spectra of products were recorded (shown in Additional file 1: Figure S1), and their melting point was determined (see Additional file 1: Table S1). The color of copper suberate (CuC8di), after staying for about a week in the open atmosphere, was changed to

a darker blue color, and the recorded infrared spectra showed a multitude of carboxylate bands at the 1600–1500 cm^{-1} region.

Melting point measurements of selected lower-chain salts were attempted by using an Electrotherma 9100 melting point apparatus. Capillary tubes (2 mm diam.) sealed at one end were loaded with a sufficient amount of the salts in powder form and then were introduced into the device. The temperature ramp was set by default at 1 per minute. At 100 °C all samples had shrunk and darkened in color, signaling a chemical transformation, which carried on at 118 °C (C6), 134 °C (C8), 175 °C (C10), 118 °C (C9di). A more detailed description of the investigated fatty acids' thermal behavior during the melting point measurements can be found in the Supplementary Information file.

Copper and copper-zinc alloy coupons and deposition of fatty acids

Copper coupons were purchased from a local machinery shop; pure copper coupons were assessed by XRF (Alloys mode, see below) to be 99.8% pure; while copper-zinc alloy coupons were assessed as 62.62% Cu, 36.72% Zn, 0.54% Al, 0.05% Cr, corresponding to a typical yellow brass alloy with a two-phase structure. In the cases where mirror-like surfaces were needed, all coupons were previously rubbed with a hydrochloric acid-moistened cotton tissue to remove the thin oxide patina and repeatedly washed with methanol; no chlorine was detected by XRF surface analysis on the cleaned surface. The coupons were subsequently polished with 4000-mesh sandpaper on a rotating polisher. In the cases of "pre-corroded" metal surfaces, similar coupons were used after exposing for at least 1 month's indoor environment at 20–25 °C and approx. 40% relative humidity without the above-mentioned steps of acid cleaning and polishing.

In both cases, copper corrosion products were assessed by FTIR spectroscopy. To assess the condition of the copper surface, spectra of both the cleaned/polished and pre-corroded metal surfaces immediately before fatty acid deposition were recorded, shown in Additional file 1: Figure S3. In the pre-corroded coupons, a weak broad maximum at 530–480 cm^{-1} due to cuprite was recorded. In the cleaned/polished coupons, these maxima were significantly weaker (Additional file 1: Figure S3).

Fatty acids were deposited on copper and copper alloy coupons from their 0.5–1.0%w/w ethanol or acetone solutions. Infrared spectra were recorded to ensure the evaporation of both solvents (approximately 1–2 min), and accordingly, consecutive infrared runs were conducted. As this method does not allow the fatty acids to be evenly spread and layered on all surfaces, all consecutive infrared spectra needed to be run on the same 3 mm-diameter circular spots, as allowed by the Bruker Alpha II aperture iris attached on the reflection accessory. On the other hand, this method allowed spectra recordings from separate spots, corresponding to spatially located deposited material of variable thicknesses.

Methods

Fourier transform infrared spectroscopy

A Bruker Alpha 2 FTIR spectrometer equipped with a DTGS detector was used, assisted with an ATR accessory (Bruker), or a reflectance accessory (Bruker), when appropriate. In certain cases, a Perkin Elmer Spectrum GS spectrometer was employed using the Spectrum v.5.3.1 software. In all cases, the used coupons (approx. 2 × 2 cm) were mirror-like by suitably polishing their surface, immediately before each run. In all cases, the blank run of the bare surface reflected its condition (weak bands of oxides were recorded in most cases, showing that oxidation occurs effectively, immediately after the polishing process producing a thin micromolecular or very thin metal oxide layer). Spectra were recorded by employing the Bruker Opus 8.5 software and recorded in reflectance mode (near-normal, or approx. 1° incident beam) at the 4000–350 cm^{-1} range. Infrared Spectra of authentics were recorded from powder samples of freshly synthesized copper carboxylates (see above) in ATR mode. Reference reflection–absorption spectra of fatty acids on gold mirror were recorded in reflection mode after their ethanol solutions were dripped on the surface and consequent evaporation of the solvent.

Normalization of spectra

For better monitoring of carboxylate formation, and following the FA consumption in a comparative manner, compensation for loss due to evaporation has been attempted in the cases of C6, C8, and C10 by normalizing on C-H vibrations that were assumed that do not change during the transformation. Normalizing at the 1480–1450 cm^{-1} region where the contribution of ($\nu CH_2 + \nu_{as} CH_3$) from both FA and metal (copper and zinc) carboxylates are observed, works satisfactorily, and was consequently applied in all relevant cases.

Kinetics through consecutive infrared spectroscopy runs

Following the acid carbonyl (i.e., carbonyl groups in carboxyl acid moieties) removal, and the carboxylate increase, time drives could be followed, resulting in kinetic graphs for all FAs. To this end, consecutive runs of infrared spectra were recorded (in most cases using the automated Repeated Measurements routine of the Opus software) with a time interval adjusted accordingly for each fatty acid, ranging from 1 min for C6 and C8, to 12 h for C10. In all cases, full spectra were

recorded at each time interval. Runs were conducted mostly at ambient temperatures, recorded by employing a commercial thermometer-hygrometer; for relatively short runs (i.e., runs ending within 2–12 h) at room temperature (air-conditioned lab space monitored by a commercial thermometer-hygrometer) was recorded within ± 1 °C; actual temperatures are reported in each case separately. In-lab relative humidity (RH) ranged between 37 and 43%. For longer runs, ranging up to a few weeks, as demanded by the higher members (C14, C16 and C18), the ambient temperature fluctuated by over ± 2 °C. For better monitoring of C14, C16 and C18, consecutive spectra were additionally recorded at 40 °C; in these cases, the metal coupons were placed on a heated plate with digital reading adjusted at the requested temperature (± 0.5 °C). In these cases, the spectra of C14, C16, and C18 (Additional file 1: Figures S4, S5, and Fig. 5, respectively) were repeatedly run, assuming that short abruptions (approx. 10') needed for the recordings do not significantly interfere with the reaction rates, typically running over 10–30 day periods. For each fatty acid on both substrates (copper and brass) multiple kinetic runs were conducted, which however, resulted in unsatisfactorily reproduced FA removal and carboxylate formation rates; this happens presumably, due to uncontrolled solvent evaporation and subsequent deposition of FAs on the metal surfaces resulting in largely uneven fatty acid 'films' which affect reactivity at a spatial level (also, see related comment in Discussion).

Blank test: control experiment on gold mirror

A blank test was run on a gold mirror to test the reactivity of FA on inert surface. Acids C8 and C10 were deposited on a 12 mm diameter gold mirror, in a similar manner to their deposition on copper surfaces. Four days after the deposition, the recorded spectrum showed only the FA with no sign of any product carboxylate.

Control experiment in the absence of oxygen

Two identical runs of caprylic acid (C8) on copper-zinc alloy coupon were conducted at 28 °C, one in the open atmosphere (C8_Air), while the other inside a closed flask under a nitrogen stream (C8_N2) and infrared spectra were recorded immediately after the FA deposition. After two hours, spectra were again recorded; C8_air showed full consumption of acid and only carboxylate spectra, while C8_N2 showed approximately 30% of remaining FA, with some amounts of carboxylates, according to spectra recorded at the initial and final times of the process.

Thickness estimation of fatty acid deposited layers on metal surfaces

The fatty acid layers, or 'films', formed after the deposition of their solutions in ethanol or acetone, construct a generally uneven multilayered structure, where the layer closest to the metal surface is assumed to be the most reactive. The layer thickness can be calculated by applying Beer's law, $A = a\ z$ for acid carbonyl bands, where A is absorbance (measured through areas under the carbonyl band), a is absorptivity, and z is the thickness in μm. Since absorptivity depends on the oscillator strength of the bond and its polarizability, carbonyl bonds belonging to the molecular layers closest to the metal surface are expected to be more polarized with higher a values, showing downshifted maxima; in the cases of C14 and C18 two acid carbonyl maxima could be recorded at ~ 1700 and ~ 1690 cm^{-1} (see Fig. 5 and Additional file 1: Figure S4), which reflect two different interaction geometries between the carboxylic moieties. Using absorptivity values of approximately 11 μm^{-1}, previously calculated [61] through correlation ($R^2 = 0.99$) of acid carbonyl infrared absorbances (areas under the carbonyl band) and ellipsometrically measured thickness values of polyethylene-acrylic acid copolymer films evenly spin-coated on copper-zinc alloy coupons. The thickness (z) values recorded in the present work were found to be between 0.3 and 6.5 μm. Representative calculated thickness values can be seen in Additional file 1: Table S2.

X-Ray fluorescence spectroscopy

X-Ray Fluorescence (XRF) spectra were acquired with a Bruker Tracer 5G XRF spectrometer, using manufacturer's 'Alloys2' calibration, in two phases; phase 1 (15 s, 40 kV, 35.4 μA, no filter), and phase 2 (45 s, 15 kV, 61.9 μA, no filter).

Experimental design for fatty acid-metal surface interaction

The interaction of fatty acid on copper metal-containing surfaces was investigated after depositing a droplet of ethanol or acetone solutions of each fatty acid on the surfaces of mirror-polished pure copper and copper-zinc alloy coupons (see Materials and Methods, 2.1.2). Infrared spectroscopy in external reflection mode was chosen as the analytical tool since it is capable of detecting the consumption of fatty acids (decrease of the acid carbonyl stretch at ~ 1700 cm^{-1}) and the simultaneous formation of the corresponding metal salts (increase of the COO^- antisymmetric stretch, ν_{as} at maxima specified in the Results section).

For this, the coupons were accordingly mounted in front of the 3 mm aperture of the FTIR system's reflection

accessory, and the kinetics of acid consumption/salt formation was followed through a specific routine of the software (see below). Subsequent spectra runs were acquired allowing the monitoring of the fatty acid-metal interaction until no further consumption of fatty acids.

(a) Samples of reference compounds in powder form were analyzed by using the Bruker Alpha II ATR accessory at 4000–400 cm^{-1}, 32 scans, and 4 cm^{-1} resolution. Consecutive spectra were recorded in all cases immediately after the deposition of the corresponding fatty acids. Kinetics graphs (Fig. 6) were composed by plotting the peak heights of the acid carbonyl maxima (acid consumption) and the antisymmetric carboxylate band (soap formation) against reaction times.
(b) The formation of carboxylates on cleaned/polished copper and copper-zinc alloy coupons was followed in reflectance mode at certain time intervals and temperatures specified for each case in the results section, by using the specific routine of Opus software. In all cases, t = 0 runs recording the initial condition of the metal surface before the addition of the fatty acid solutions (see above) were carried out; in all cases, a null spectrum suggesting that no oxides were present was obtained. Spectra in all cases are shown after baseline correction, but no further treatment. To highlight the effect of copper corrosion products (i.e., copper oxides) additional experiments were done by depositing fatty acids on pre-corroded copper and copper-zinc alloy coupons; the presence of oxides is demonstrated, by running blank runs of all surfaces immediately before acid deposition; spectra are shown in Additional file 1: Figure S2.
(c) The control experiment in the absence of oxygen was conducted at 28 °C by employing a copper-zinc alloy coupon after depositing the C8 acid. After recording the infrared spectrum (t≃0), the coupon was immediately placed in a glass bottle with a modified lid having an inlet and outlet allowing the flow of N_2 gas; the reaction was interrupted after 120 min, which corresponds to the approximate time of full consumption of this specific acid in an oxygen atmosphere; the infrared spectrum was accordingly recorded.

Results

In this study, FA were deposited from their ethanol or acetone solutions on mirror-like surfaces of 99.5% pure copper and brass (63.88% Cu—36.05% Zn 'yellow' brass alloy) coupons and the interaction phenomenon involving the transformation of the former was consecutively recorded with transflection infrared spectroscopy. All the infrared maxima observed through this process, as well as their assignments, are listed in Table 1. The infrared spectra of fatty acids in the bulk have been previously reported [13, 66–69]. Furthermore, spectra of fatty acid carboxylate authentics, synthesized for the purposes of this work, are shown in Additional file 1: Figure S1, while their infrared maxima and assignments are listed in Additional file 1: Table S1. As our results regarding fatty monoacids (FMA) are different from those of fatty diacids (FdiA), they are presented separately.

Interaction of fatty monoacids with copper and copper alloy surfaces

The products formed through the interaction of FMA C6, C8, C10, C12, C14, and C18 with mirror-polished copper and copper alloy surfaces were investigated by depositing droplets of their ethanol or acetone solutions. The chemical interactions between FA and the copper surfaces were followed through infrared spectroscopy focusing on the carboxylic (acidic C = O, see above) and carboxylate bands (mainly, the ν_{as} of COO^-). The carboxylate group shows two bands, one assigned to the antisymmetric stretch (generally, a strong absorption at ~ 1600–1500 cm^{-1}) and another to its symmetric stretch (generally, weaker at ~ 1420–1380 cm^{-1}).

A white-pale blue sediment was evident by visual inspection of C6, C8, and C10 within 1–2 h after deposition on all coupons. As shown in the consecutive infrared spectra of Figs. 1, 2, and 3 respectively, the FMAs were gradually consumed with the simultaneous formation of the corresponding carboxylates, while carboxylate bands appeared in all trials in copper and copper-zinc alloys. For these specific acids, consumption was faster than the formation of carboxylates, while their final intensities were significantly weaker than the simultaneously decreased acid carbonyl ones, suggesting effective evaporation of the lower FA within the time frame of the entire transformation (cf. melting points in Additional file 1: Figure S1).

For C6 on the pure Cu surface, in particular, evaporation was too fast for any reaction product to be recorded, while on the copper-zinc alloy surface, carboxylates were recorded immediately after deposition, while the C6 acid carbonyl was consumed within 30 min; beyond that time, only weak carboxylate bands are evident). For C8 and C10, evaporation is slower occurring within ~ 2:30 h, and 4 h, respectively. The prominent antisymmetric stretch of copper carboxylate bands was recorded in both types of metal coupons at ~ 1585 cm^{-1}, with a minor one at 1520–1515 cm^{-1}. On the other hand, on copper-zinc alloy coupons, a single zinc carboxylate band at 1526 cm^{-1} is observed for C6 (Fig. 1), two bands at ~ 1550

Table 1 Main infrared peaks of fatty acids and copper carboxylates on clean/polished copper and copper-zinc alloy coupons

Fatty acids	Cu carboxylates[1], cm^{-1}	Zn carboxylates[2], cm^{-1}	Assignments	Notes[3]
~3100 (br)	–		*v*OH	Typically, very broad
2960–2956	2954	2956	$v_{as}CH_3$	Only in monoacids and their carboxylates Marginally variable, according to number of carbons in acids
2934–2919 2977–2911	2930 (C6); 2920 (C8); 2014 (C10-C18)	2940(sh), 2926–2916 (C6-C18)	$v_{as}CH_2$	Generally, CuC and ZnC down-shifted with respect to parent FAs General trend: variable, according to the number of carbons
2991, 2951, 2941, 2911 (C8di) 2977, 2937, 2915 (C9di)	2964, 2943, 2931, 2917, 2906 (C8di) 2942, 2927, 2909 (C9di)	2964, 2943, 2931, 2917, 2906 (C8di) 2842, 2927, 2906 (C9di)		Multiplets in diacids and corresponding carboxylates; higher multiplicity for C8di
2875–2872	2871	2870	v_sCH_3	Variable, according to the number of carbons
2851	2853 (C6); 2851 (C8); 2848 (C10-C18) 2851 (C8di) 2849 (C9di)	2850	v_sCH_2	Variable in CuC according to the number of carbons
2670, 2565 (FMA)	–	–	*v*O-H•••O=C (dimer band stretch)	Only in FA, often used diagnostically; weak, structured with shoulders
2759, 2676, 2599, 2534 (C8di) 2774, 2698, 2621, 2553 (C9di)				More extended in diacids
1714 to 1690 (C6, C8, C10, C12)			*v*C=O, acidic	In C6–C12: single bands, maxima down-shifted upon acid consumption and film thinning
1700, 1688 (C14, C18)				In C14, C18 doublet at fixed maxima during the FA consumption
1692–1690				In C8di, C9di
	1616–1613 w (C6-C10)		$v_{as}COO^-$	Intermediate band in copper carboxylates of C6-C10
	1583 (C6)	1527 (C6)		
	1583 (C8)	1548, 1525 (C8)		
	1581, 1519 w (C10)	1550, 1532–1524 (C10)		
	1585, 1525–1519 w (C12)	1537 (C12)		
	1585 (C12)	1537 (C14)		
	1586 (C18)	1540 (C18)		
	1589 (C8di)	1552, 1532 (C8di)		Diacid carboxylate bands in both substrates were observed on pre-corroded surfaces
	1600 (C9di)	1552, 1527 (C9di)		
1465, 1416	1458, 1415	1468, 1456	δCH_2 scissoring	FA: Split into two components (two in diacids)
1457 (?)	1439(?)	1439(?)	$\delta_{as}CH_3$	Barely distinguishable in Cu and Zn carboxylates
1436			$\delta_{ip}COH$	Relatively broad
	1440–1431	1400–1396 (br)	v_sCOO^-	Generally medium-weak intensity for most carboxylate bands; relatively sharp
	1400 1395			Intermediate (C8, C10) C8di and C9di
1382	n.d	n.d	δ_sCH_3 ('umbrella' vibration)	
1356–1347	1366, 1341,	1366, 1341,	*τ*CH2	Splitting in progression bands for monoacids in their crystalline state (at room temperature, higher than C10);
1318–1185	1312–1185	1312, 1207	*w*CH2	In crystalline, saturated monoacids and diacids progressions
1108			*v*C–OH	Up shifted for longer hydrocarbon chains. Weak or not observed for diacids
943–935 (br)			δ_{oop}C–O–H•••O=C	The dimer bending band; characteristic of fatty acids
720, 800–607	720	720	*ρ*CH2	Stronger in long hydrocarbon chains; the 725 cm^{-1} peak doubly split in crystalline monoacids

Table 1 (continued)

Fatty acids	Cu carboxylates[1], cm^{-1}	Zn carboxylates[2], cm^{-1}	Assignments	Notes[3]
690			δ_{oop}C–O–H	Overlapped in unsaturated acids

FA fatty acids, *FMA* fatty monoacids, *FdiA* fatty diacids, *MC* metal carboxylates, *CuC* copper carboxylates, *ZnC* zinc carboxylates

[1] Maxima values from both copper and copper-zinc alloy coupons

[2] Maximum values from copper-zinc alloy coupons

[3] Notes adapted from [13]

v: stretching vibration; v_s symmetric stretching; v_{as} antisymmetric stretching; *δ*: bending vibration; δ_s symmetric bending; δ_{as} antisymmetric bending; δ_{ip}: in-plane bending; δ_{oop}: out-of-plane bending; *τ*: twisting vibration; *w*: wagging vibration

and ~ 1535 cm^{-1} appeared for C8 and C10 (Figs. 2, and 3 respectively), and a single band at 1537–1540 cm^{-1} for C12 (Fig. 4), C14 (Additional file 1: Figure S4) and C18 (Fig. 5); maxima and assignments are listed in Table 1.

For C6, C8, and C10, a band at 1614 cm^{-1} was initially recorded, which was gradually decreased to form the final copper carboxylate bands (spectra of Figs. 2a, b, 3a, and b). The isosbestic points between the consecutive curves of the two carboxylates suggests that the 1614 cm^{-1} transient band is possibly due to an intermediate copper carboxylate species, which will be discussed in the next Section. In support of the above, indicative kinetics curves are presented showing the decrease of the starting materials (i.e., FAs), the formation of carboxylates, as well as the intermediacy of the above-mentioned transient species (see Additional file 1: Figures S2a for C6, and Additional file 1: Figure S2b and Additional file 1: Figure S2c for C8).

Interestingly, no similar intermediate was evident in the runs conducted for the higher acids. More particularly, the main features in the reactivity of C12, C14, C16, and C18 with both copper-zinc alloy and pure copper surfaces (Figs. 4, 5, Additional file 1: Figures S4 and S5) showed (a) significantly lower kinetics (as indicatively shown in Fig. 6), and (b) the absence of any intermediate species. Indicative consumption times of reactants on copper alloy surfaces at around ambient temperatures can reach approximately, 16 h (C12), 6 days for C14, up to 30–40 days for C18 (Table 2). In all cases, the copper carboxylate antisymmetric vibration is observed at ~ 1585 cm^{-1}, while the symmetric one, at 1440 cm^{-1}.

Since the evaporation phenomenon interfered with the chemical consumption of the lower acids, compensation for loss due to evaporation has been attempted by normalizing on C–H vibrations, assuming that their absorbances do not change upon the transformation from acid to carboxylate (see Materials and Methods, 2.2.2). This technique allowed for comparative monitoring of the acid carbonyl consumption and the carboxylate formation, thus offering indicative reaction rates. The above are highlighted as an example in Fig. 2c, d (showing the normalized spectra for C8) which can be compared with Fig. 2a, b (original spectra). In the kinetics shown in Fig. 6, it is evident that the consumption of C12 is significantly slower than that for C6, C8, and C10, without the formation of an intermediate. The consumption of C8 and C10 during the time frame of the intermediate presence is slower, as shown in Fig. 2e, f, while it becomes faster as it transforms into the final carboxylate.

Regarding higher FAs, myristic acid (C14) is consumed in 2.5–5.5 days, also without any intermediate. For the higher members, reactions were followed at 40 °C (see Materials and Methods, 2.2.3); in particular, palmitic (C16, Additional file 1: Figure S4), and stearic acid (C18, Fig. 5) show similar reactivities and are completely transformed to their corresponding carboxylates on both types of surfaces after 20–24 days (Table 2).

Fatty diacids on copper and copper alloy surfaces

The FdiA, such as azelaic (C9di) and suberic (C8di) have attracted special attention among researchers, as they are markers of the oxidative degradation of unsaturated lipids in oil paintings and of fatty substances as organic residues contained in archaeological vessels [10–12, 14, 47, 71, 72]. However, their carboxylates in general have received little attention.

The carbonyl maximum of both diacids on copper and copper alloy surfaces appears at 1693–1691 cm^{-1} relatively lower than the corresponding authentics [13]. Furthermore, a comparison of their reactivity on clean/polished metal surfaces under identical conditions with those of monoacids showed negligible consumption of the acids after their deposition. In particular, suberic acid showed weak carboxylate maxima with its infrared intensity of the carboxylate bands not further increasing after a few hours (Fig. 7a, b, lower part). Azelaic acid formed no copper carboxylate within the same time period, while weak zinc carboxylate bands at 1547 and 1527 cm^{-1} were detected in the copper-zinc alloy coupons, which did not further increase (Fig. 8a, b, lower part).

On pre-corroded coupons left in the open atmosphere for several weeks), immediately upon deposition both suberic and azelaic acids formed their copper

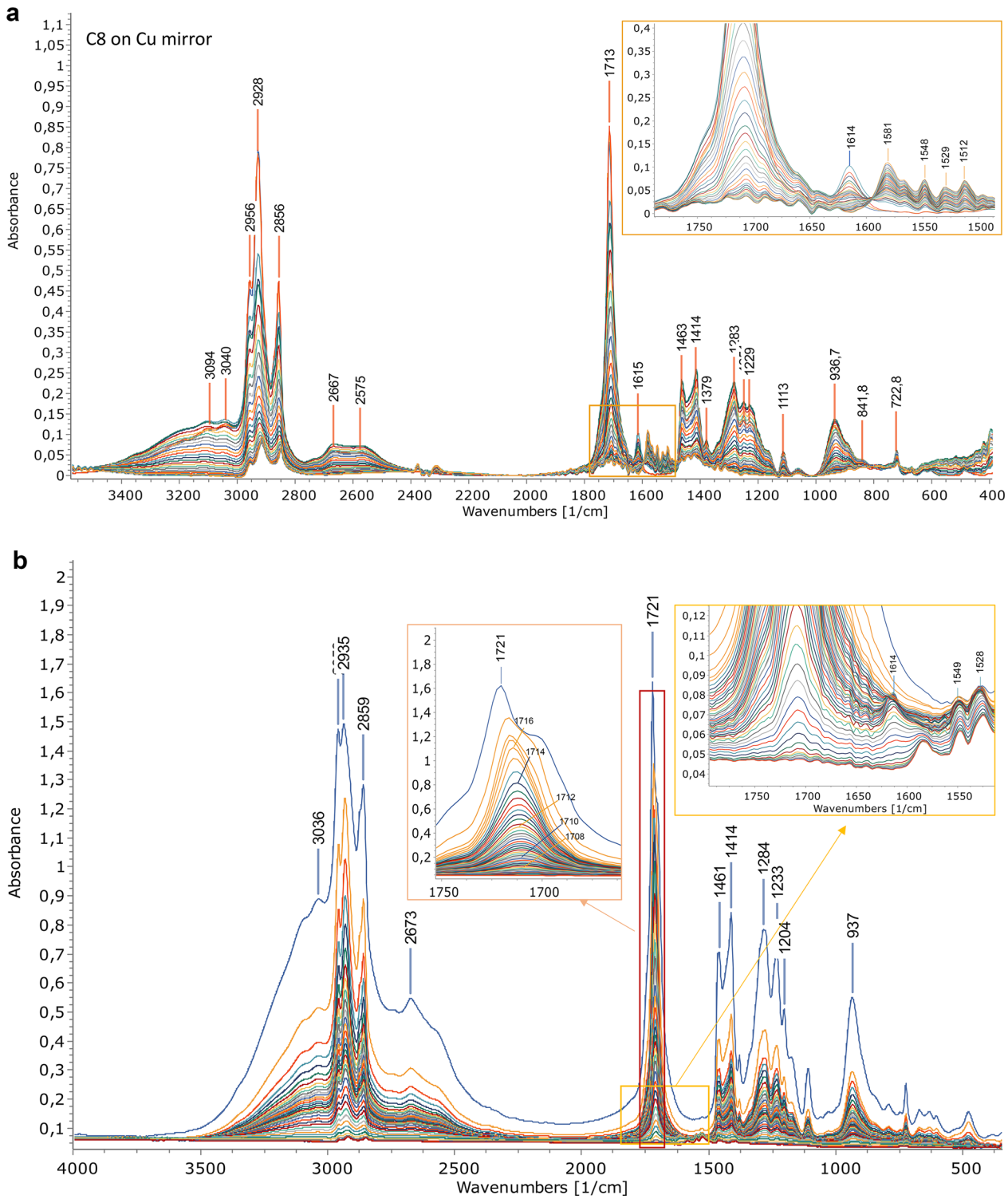

Fig. 2 Consecutive spectra of caprylic acid (C8) after deposition on **a** pure copper surface and **b** copper-zinc alloy surface; insets: zoom in the carbonyl-carboxylate region. The region 1780–1480 cm^{-1} from the spectra after compensation for loss due to evaporation of C8 after deposition on **c** pure copper surface and **d** copper-zinc alloy surface (see Materials and Methods, 2.2.2). In all cases, consecutive spectra were recorded at ~ 20 °C and RH 40%; time in (**c**) is given in hours:minutes

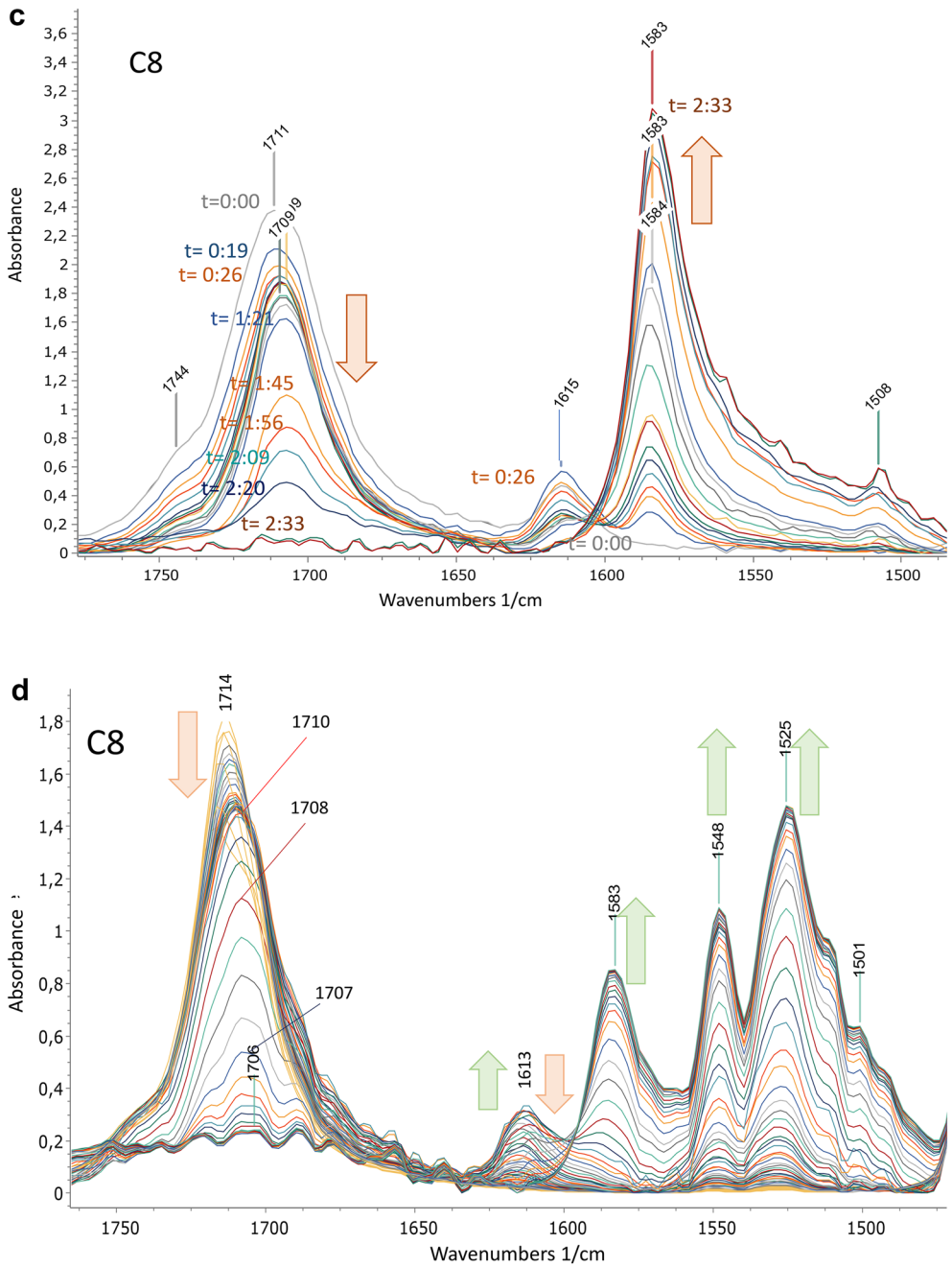

Fig. 2 continued

carboxylates (1589 cm^{-1}) on pure copper surfaces and both the copper and zinc carboxylates (1552 and 1532 cm^{-1} for the latter) on copper-zinc alloy, as shown in Figs. 7a, b and 8a, b, upper part, respectively. The infrared band maxima were close to those of the corresponding authentics [13]. Importantly, in all cases, the corresponding fatty acids did not further consume, and consequently, the carboxylate bands did not further increase. Cleaning the coupon surface with ethanol removed all diacid quantities and left clean, mirror-like pure copper and copper-zinc surfaces, with infrared spectra similar to those of the coupons before the deposition.

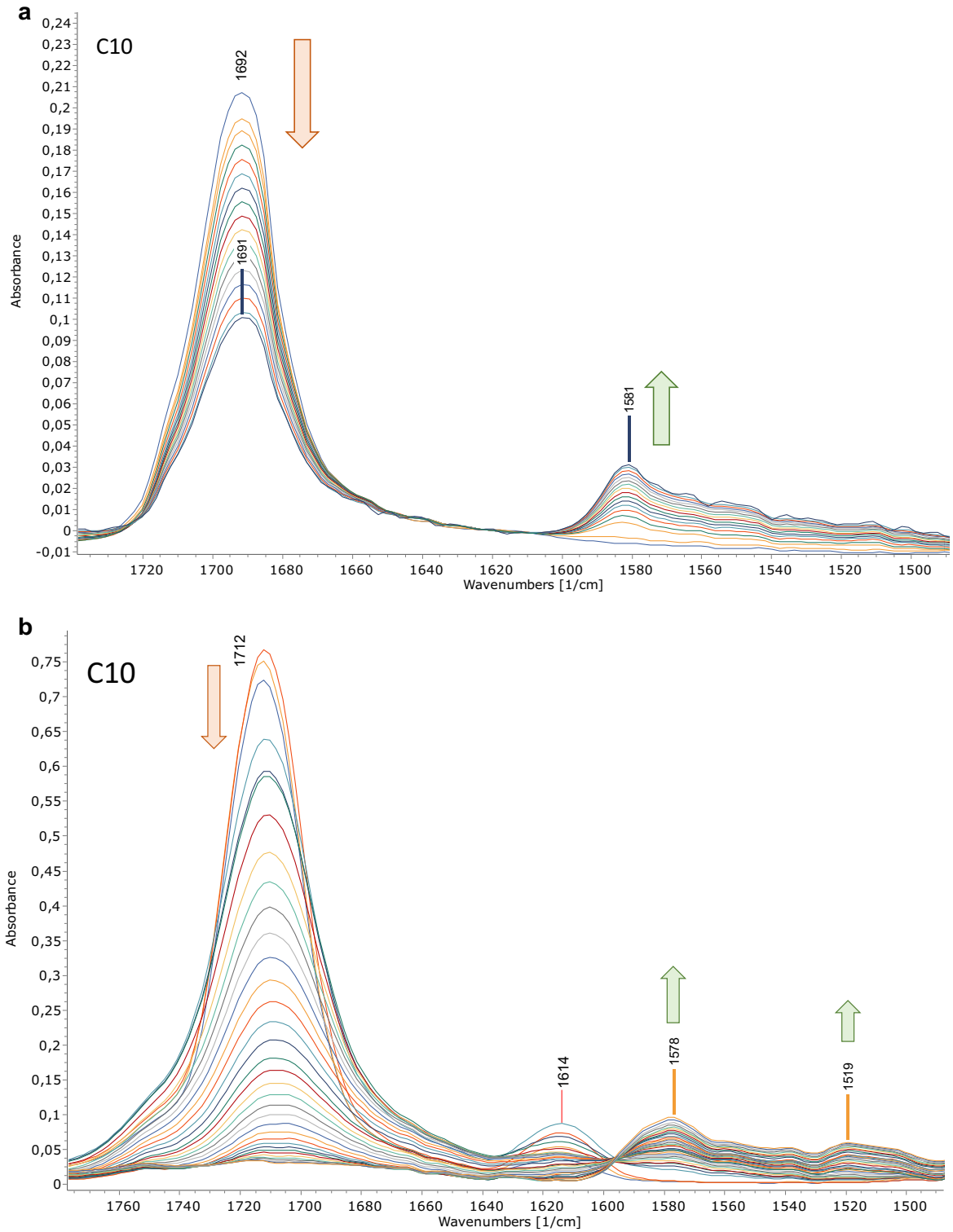

Fig. 3 The region 1800–1500 cm^{-1} from consecutive spectra of C10 after deposition **a** and **b** on pure copper surface, and **c** and **d** on copper-zinc alloy surface; spectra on **a** and **c** correspond to clean/polished surfaces, while **b** and **d** to pre-corroded surfaces. Runs were recorded at 20 °C and RH 40%

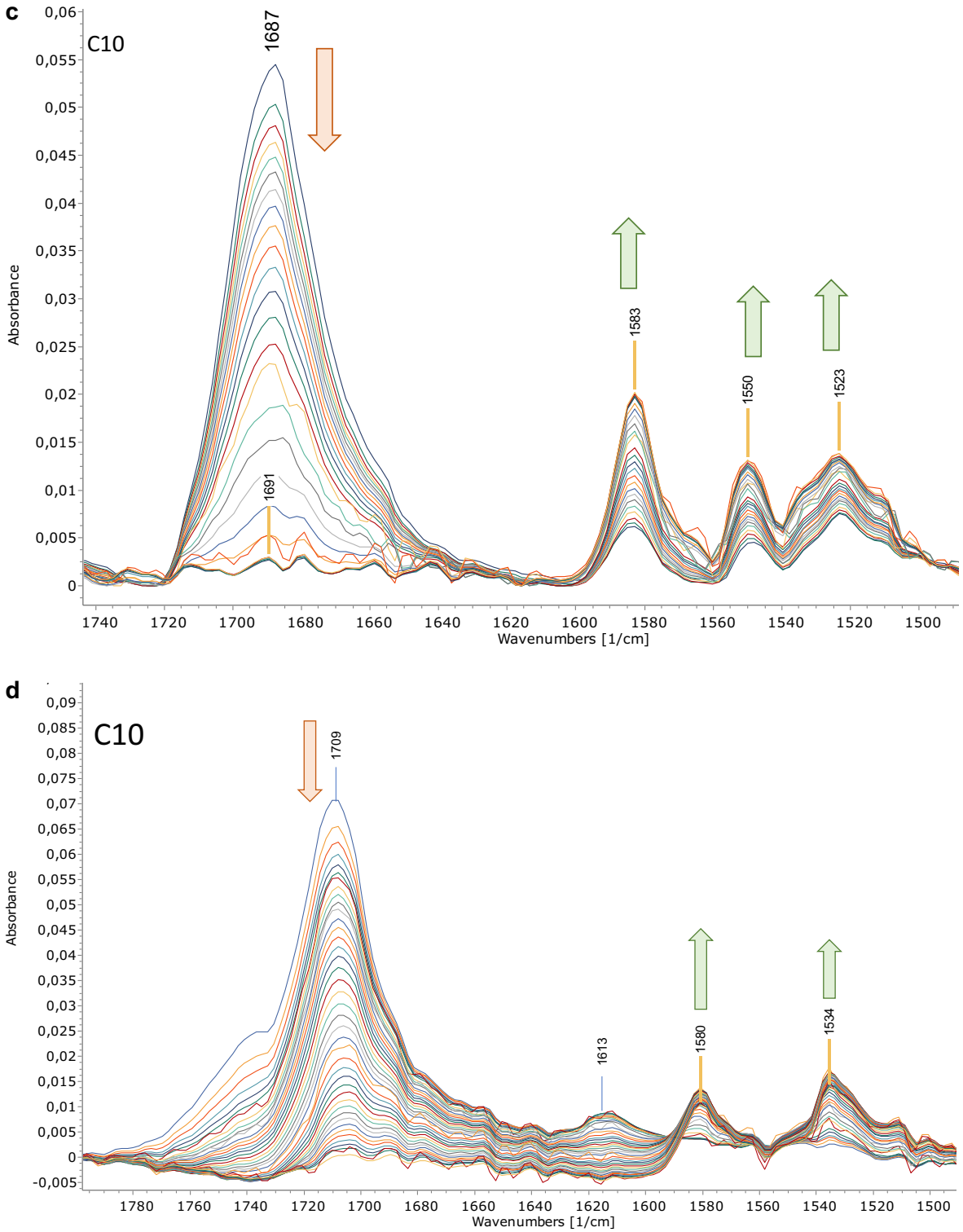

Fig. 3 continued

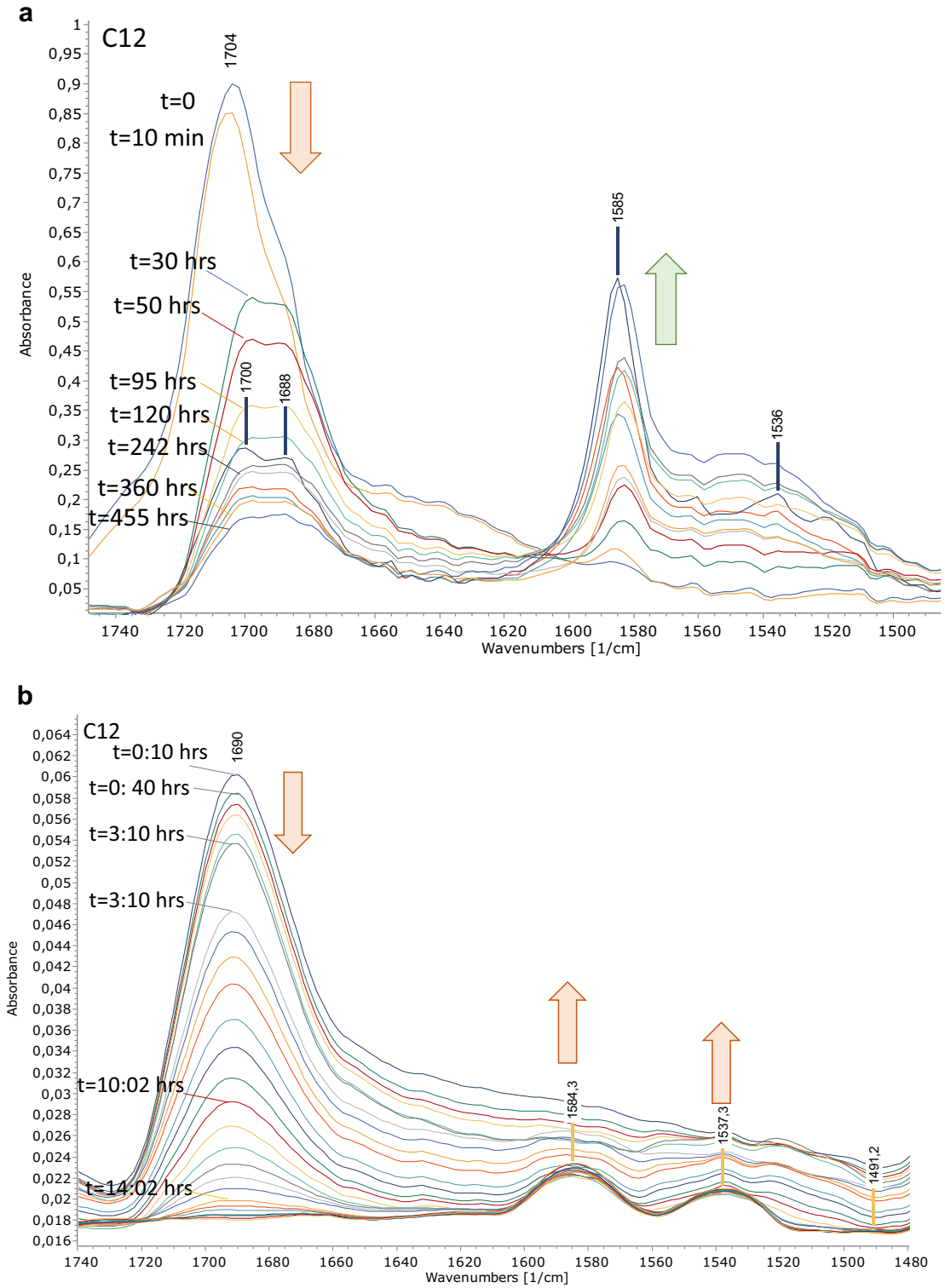

Fig. 4 The region 1740–1480 cm^{-1} from consecutive spectra of lauric acid (C12) after deposition on clean/polished **a** copper and **b** copper-zinc alloy surfaces. Runs were recorded at 20 °C and RH 40%

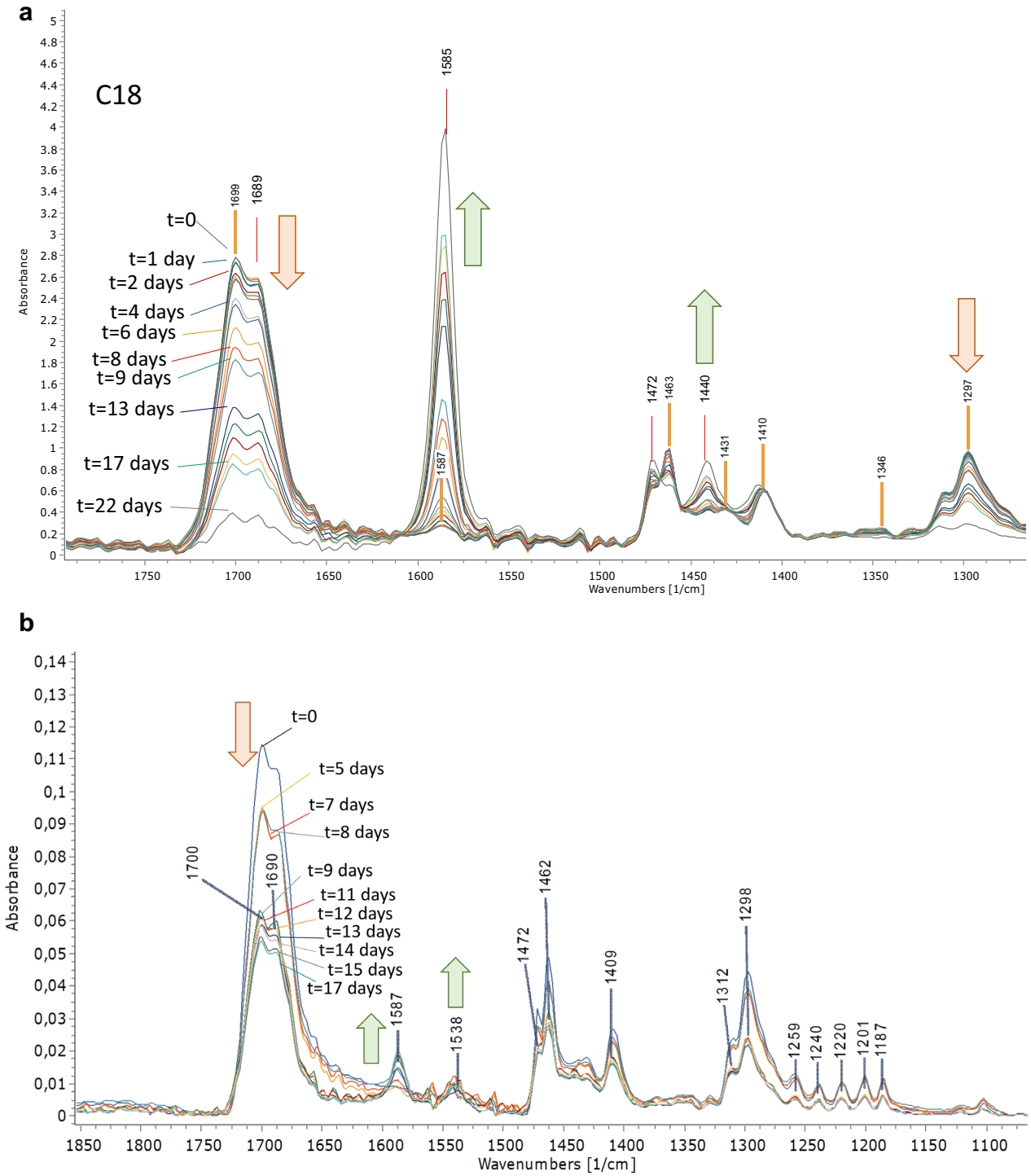

Fig. 5 The regions 1800–1200 and 1800–1100 cm^{-1} from consecutive spectra of C18 after deposition on clean/polished surfaces **a** pure Cu and **b** Cu–Zn alloy

Discussion

The interface between the FA and the copper-containing metal surface depends on their chemical nature and is affected by factors such as the atmospheric oxygen, moisture, and the existence of metal oxide films. As a general remark, in all cases, FA deposited on the

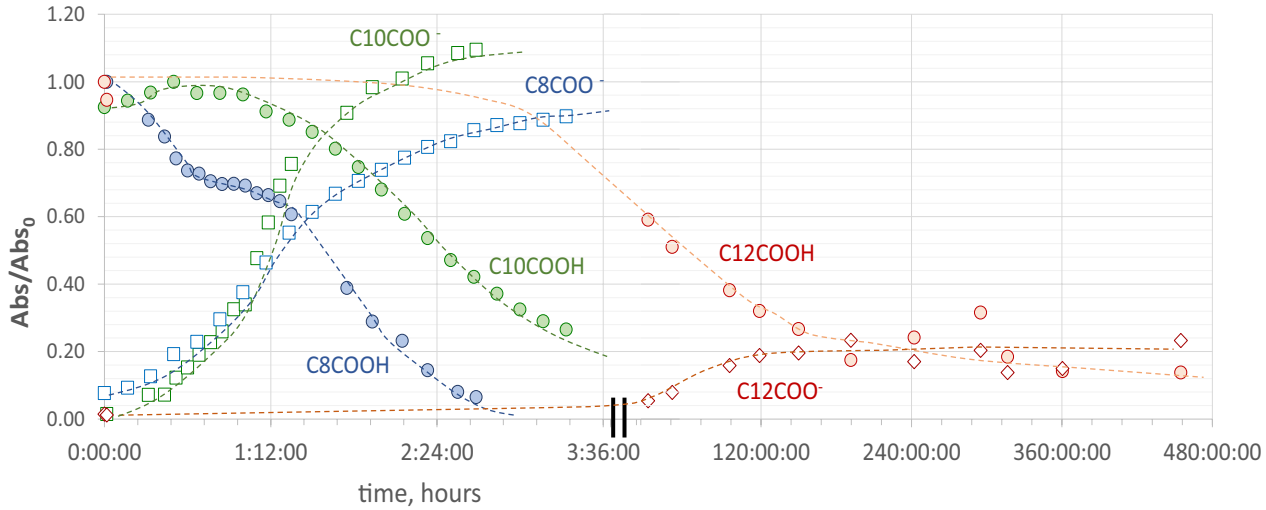

Fig. 6 Time drive of the C8, C10, C12 carboxylic acid removal and carboxylate bands formation on clean/polished pure copper surface; data from maximum height values of acid carbonyl and carboxylate maxima after consecutive infrared runs (see main text). Values in C8 and C10 are reported after previous compensation for acid evaporation. For all acids, representative runs are shown, (see Materials and Methods)

Table 2 Main spectroscopic data and reaction times of FMAs on pure copper and copper-zinc surfaces

Acids	m.p., °C [a]	Cu		Cu–Zn		Notes
		Consumption time [b]	Carboxylate maxima (v_{as}, cm^{-1})	Consumption time [b]	Carboxylate maxima (v_{as}, cm^{-1})	
C6	−3.2	–	n.d	35 min (25 °C)	Cu: 1612 (w, int.), 1582 Zn: 1526 (s)	Evaporation of FA is sufficiently fast, interfering with reaction; consumption rate is lower in the first stages that the intermediate at 1614 cm^{-1} is produced
C8	15.4	2 h 50 min (25 °C)	1612 (w, int.), 1584 (s), 1510 (w)	> 1 h (13 °C) ~ 50 min (28 °C)	Cu: 1612 (w, int.), 1582 Zn: 1526 (s)	
C10	31.0	3 h 40 min (20 °C)	1615 (vw, int.), 1581 (s), 1510 (w)	4 h (19 °C)	Cu: 1612 (w, int.), 1586 (s) Zn: 1550 (m-s), 1523 (m-s)	Evaporation of FA interferes with reaction
C12	44.8	~ 8 days (20 °C)	1582 (s), 1512 (w)	14 h (20 °C)	Cu: 1585 (s) Zn: 1537 (s)	After forming the first carboxylate amounts, no other compounds or intermediates were formed
C14	54.4	~ 5.5 days (20 °C)	1586 (s)	2.5 days (20 °C)	Cu: 1584 (s) Zn: 1537 (s)	
C16	62.9	> 18 days (40 °C)	1585 (s)	~ 24 days (40 °C)	Cu: 1584 (s) Zn: 1539 (s)	
C18	70.1	> 20 days (40 °C)	1585 (s)	~ 20 days (30 °C) ~ 15 days (40 °C)	Cu: 1587 (s) Zn: 1539 (s)	

[A] values from [70]

[B] indicative times (see Materials and Methods, 2.2.3)

v_{as}antisymmetric stretch

s strong, *m* medium, *w* weak, *vw* very weak, *int.* intermediate

surfaces of both pure copper and copper-zinc alloy interact with the metal surface and form the corresponding metal carboxylates. The phenomenon is followed by both the consumption of the parent acid (carbonyl infrared bands) and the formation of the products (carboxylate bands). As a control, a similar deposition of fatty acids on gold mirror-like surfaces did not produce any carboxylates, due to the inertness of gold (see Materials and Methods, 2.2.4).

Most spectra bands of the carboxylate products correspond to the reference spectra of copper carboxylates (as shown through the synthesis presented in the experimental section of this work) and zinc carboxylates [13]. Generally, well-crystallized metal soaps show sharp

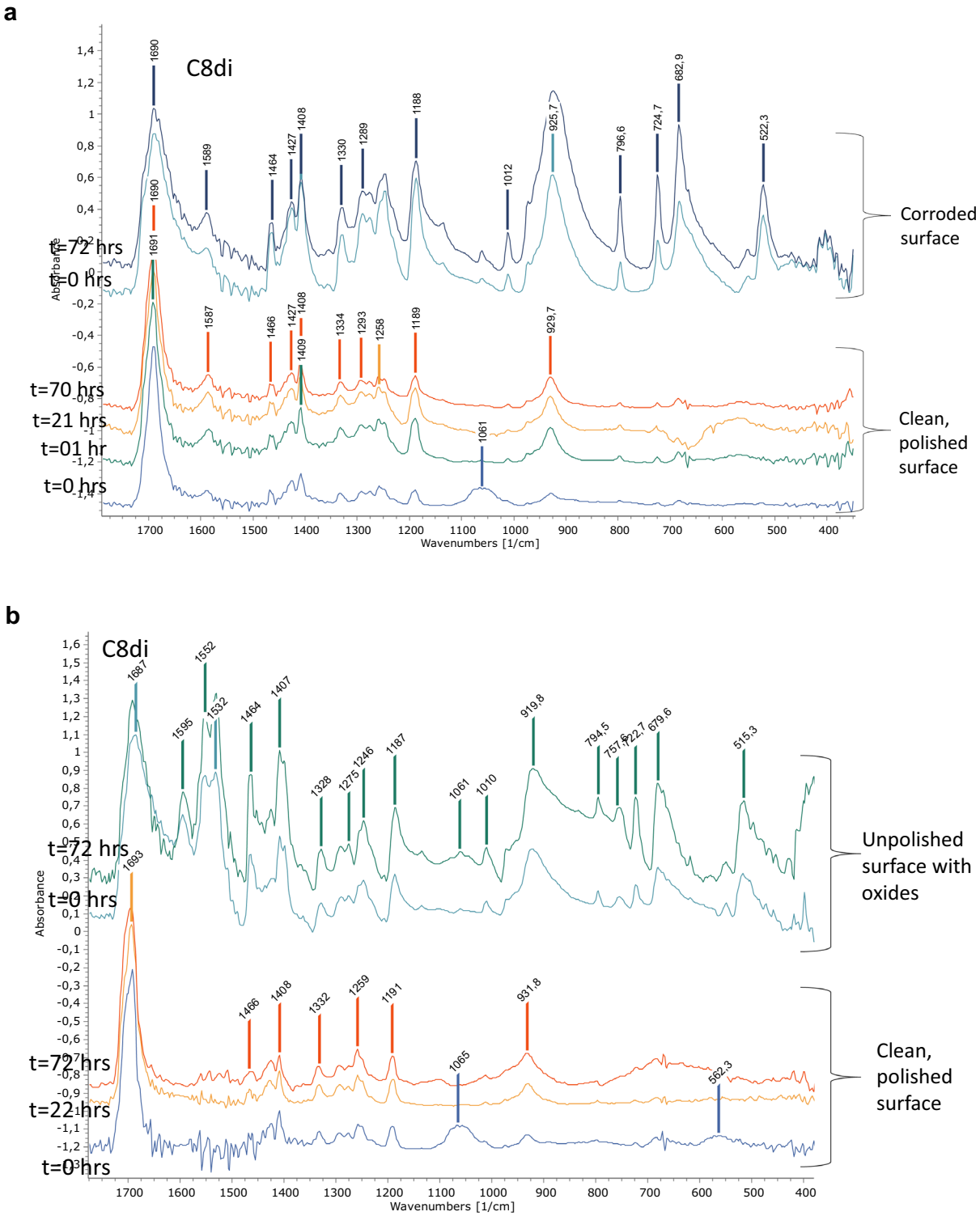

Fig. 7 Spectra zoomed in the region 1750–400 cm^{-1}, of suberic acid (C8di) at various time intervals after deposition on **a** pure copper surface and **b** copper-zinc alloy surface. Lower part in each image: clean/polished surfaces; upper part: mildly corroded surfaces

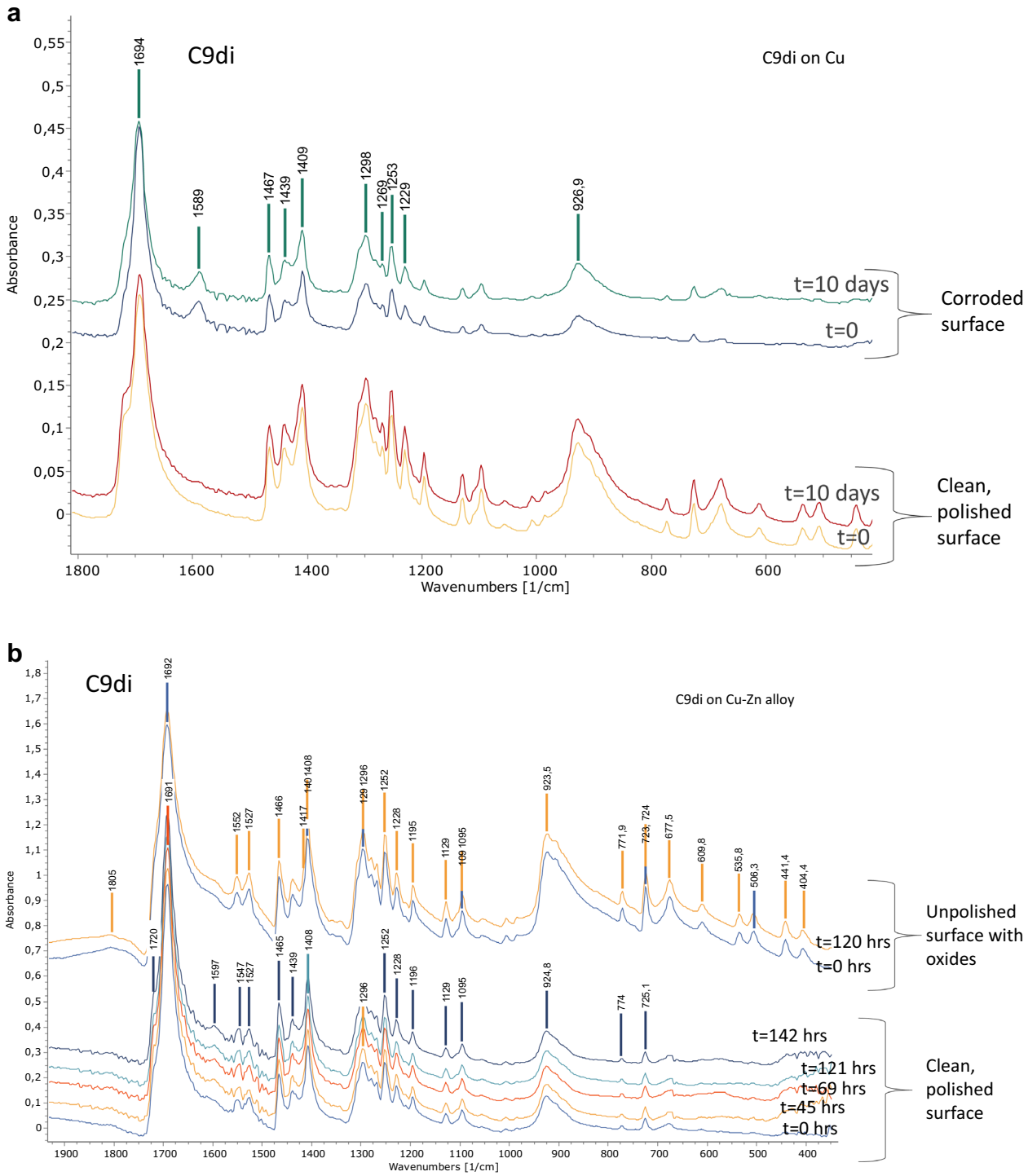

Fig. 8 Spectra zoomed in the region 1750–400 cm^{-1}, of azelaic acid (C9di) at various time intervals after deposition on **a** pure copper surface and **b** copper-zinc alloy surface. Lower part in each image: clean/polished surfaces; upper part: mildly corroded surfaces

bands, while broad line shapes generally denote amorphous regions, due to complex mixtures. The main copper carboxylate maximum shows the antisymmetric peak at 1580–1586 cm^{-1} and the symmetric one at 1415 (C_8) and 1424 cm^{-1} (C_{10}-C_{18}) with Δ at ~ 157–168 and cm^{-1} (see values for the authentics in Additional file 1: Table S1) which has been assigned to a bridged bidentate dimer with a geometry resembling that of a paddle-wheel

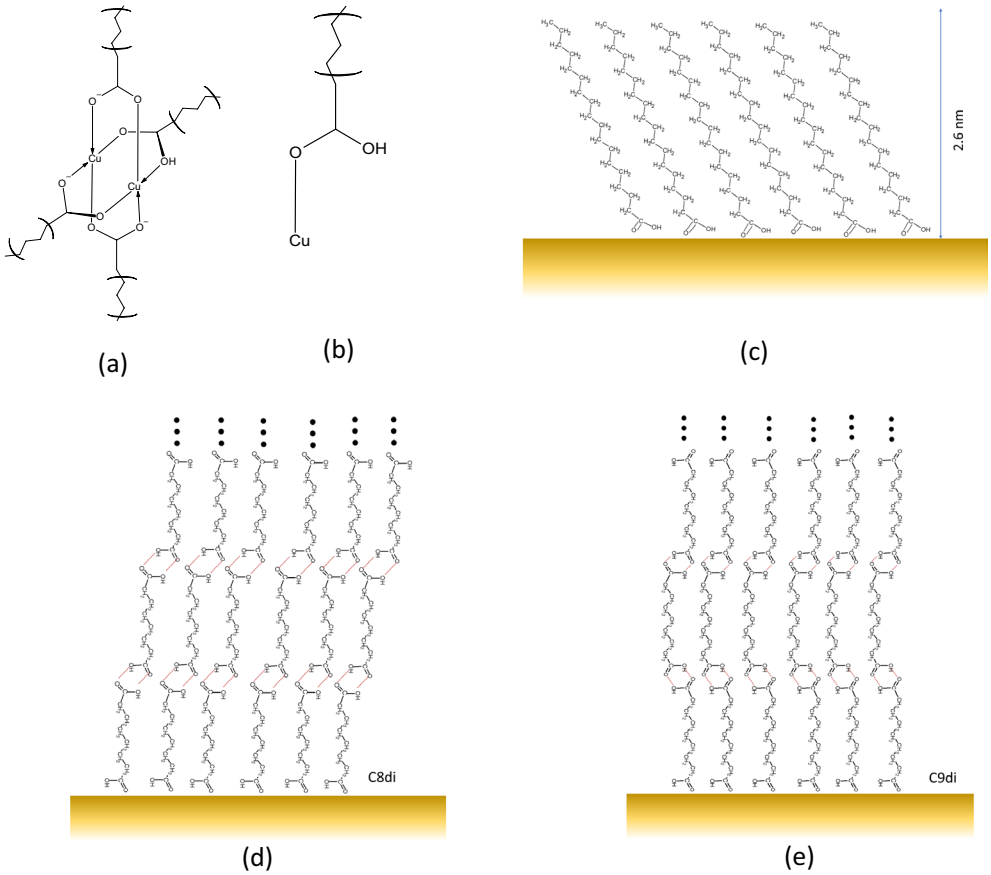

Scheme 1 Chemical structures of **a** binuclear paddle-wheel bidentate bridged complex (adapted from [91]); **b** unidentate copper complex. Organized FMA and FdiA structures on copper surfaces: **c** monolayer of a tilted-geometry array of C18 molecules (adapted from [42]); possible multilayer structures of **d** C8di and **e** C9di on copper or copper alloy surfaces

[54, 55], shown in Scheme 1a. Besides, the line shape of the carboxylate bands depends on the crystallinity of the soap, which may variably depend on the surrounding medium [23, 24, 73]. At this point, based on the fact that excellent crystals are formed during the processes studied in this work, it should be noted that future work involving X-Ray diffraction data to straightforwardly compare with infrared results and particularly, with symmetry considerations and the Δ value is needed.

Reactivity and the intermediate

One of the findings of this research is the variation in FA consumption and carboxylate formation rate depending on their alkyl chains. For the lower FA, compensation for evaporation was necessary through normalization, which allows the study of the chemical process alone, and also the better comparative monitoring of all species. The infrared subsequential runs showed that C6, C8, and C10 (liquids in the temperature of these experiments) were consumed considerably faster than the rest of the monoacids (solids); this was also visually confirmed. Caproic acid (C6, m.p. -3 °C), which has the shortest alkyl chain among those investigated, shows the fastest consumption, which however, evaporated at room temperature posing difficulty for its monitoring; evaporation was slower for caprylic (C8, m.p. 16.5 °C) and capric (C10, m.p. 31.4 °C) acids. Nevertheless, on average, their product formation rates were found to decrease as alkyl chain length increases.

Respectively, consumption of the corresponding FA followed after compensation for evaporation through spectra normalization (See Materials and Methods, 2.2.2), occurred in a matter of a few hours in near ambient temperatures on both types of surfaces, as shown in Table 2, and Fig. 6, and Additional file 1: Figure S2. The decrease of the acid carbonyl band (Fig. 2e, f for C8) during the time drive shows first, a slow part for the lower acids occurring almost simultaneously within the time frame of the 1614 cm^{-1} intermediate, followed by a faster section until its full consumption.

The intermediate at 1615 cm^{-1} is another interesting result of this study. An analogous band at 1620 cm^{-1} has

been previously reported in the case of an ethyl acrylic acid co-polymer, which was generally assigned to a copper acrylate coordination complex [61]; this band was more prominent in the case of heavily corroded copper coupons bearing copper oxides (cuprite, Cu_2O, and tenorite, CuO). The fact that this same band is also formed in unpolished copper surfaces in this study, leads to the conclusion that this is also a carboxylate, possibly a substitution product of FA and cuprous oxide (cuprite, Cu_2O), and, therefore, this most possibly refers to a copper(I) carboxylate. Furthermore, considering the symmetric stretch maximum at 1396 cm^{-1} for the intermediate, the high Δ value (~ 215 cm^{-1}) of this carboxylate band suggests a low-symmetry unidentate coordination [50, 52, 74], which could be explained by the Cu(I) complex. In copper-zinc alloys, zinc is also oxidized in the presence of oxygen and humidity to zinc oxide (ZnO), and therefore, similar reaction schemes may explain the zinc carboxylates at 1530, and 1560 cm^{-1}.

An additional difficulty concerned the reproducibility of kinetic runs, after being attempted in multiples. In addition to the evaporation phenomenon for C6, C8, and C10 (mentioned above), the lack of random encounters between fatty acids and metal sites available for the reaction is a crucial factor, responsible mostly for the higher-m.p. members, which are solid at ambient temperature. It should be kept in mind that in the case of kinetics in solutions, encounter and heat exchange randomness is well-obeyed, and therefore reaction rates under similar concentrations, temperature, and pressure can be satisfactorily reproduced [75]. On the other hand, reactions at solid–solid interfaces, such as the mid- and higher-FA-metal interface are controlled by the molecular packing and contact at the interface between the generally immobile reagent molecules or ions [76]. Besides, the variability of 'film' thicknesses (majorly influenced by immediate solvent evaporation after dripping the fatty acid solution on the metal surface) is an added factor that needs to be controlled. Under our repeated kinetic runs, even though temperature and FA concentrations in dripped solutions were kept under control, fatty acids were unevenly deposited on the surfaces, so that areas of higher FA thickness suggest more molecular layers on the flat metal surface. As a result of the gradual consumption of the lower-lying FA layers, metal sites are partly covered with newly-formed carboxylates, and are therefore, less available for reacting with the overlying FAs; this may result in a non-uniform propagation of the overall reaction. At this point, the need for reproducible conditions needs to be addressed, among others, involving the study of unimolecular FA 'films' on copper and copper-zinc alloy surfaces and following their reaction rates towards copper and zinc carboxylates. As a result, only 'representative' kinetics, are presented in this work, which however demonstrate the reactivity differences between the various FAs.

The higher acids, lauric, myristic, and stearic, are reacting considerably slower reflecting the molecular mobility; stearic acid (m.p. 70.1 °C) for instance, at moderately elevated temperatures (Table 3) reacts within 25 days on the pure copper surface and 8 days on the copper-zinc alloy surface, while its full consumption is projected to reach ~ 40 days in room temperature (comparing Additional file 1: Figures S5 and Table 3). The lower reactivity of the higher FA can be linked (a) to their restricted molecular mobility (depending on alignment and hydrophobic associations among alkyl chains [13, 77], and the consequent orientation of the polar carboxyl end towards the metal surface with a tilted molecular geometry (~ 15° angle with respect to the normal) [39, 42, 43]), and (b) to their lower acidities (pKa values of 4.8–5.0 for short chains may reach 8–10 for C16 and C18, also controlled by chain lengths and interchain distances upon packing, as well as the chemical nature of the interface [78, 79]). This allows a self-assembled monolayer (SAM)-type formation that may offer a temporary protective layer, finally resulting in a decrease of the reaction rate [42, 43].

$$Cu + {}^1/_2O_2 + H_2O \rightarrow Cu^{2+} + 2OH^- \quad (1)$$

$$RCOOH + OH^- \rightarrow RCOO^- + H_2O \quad (2)$$

$$2RCOO^- + Cu^{2+} \rightarrow (RCOO)_2Cu^{(II)} \quad (3)$$

Equations (1–3) explain the cupric carboxylates (infrared maximum at 1585–1580 cm^{-1}) gradually building from all FA through the electrochemical processes (1–3). At the first level, the intermediacy of oxygen is necessary for the overall process, as shown in a controlled experiment for C8 under nitrogen purging (see Materials and Methods, 2.2.5). Given, also, that a thin film of cuprite (Cu_2O) is instantly formed through an electrochemical process on the copper surface when exposed to oxygen (Eq. 4), this oxide may react with FA according to the substitution reaction of Eq. 6. It needs to be pointed out that no copper oxides could be detected during the course of the reactions; the use of Raman Spectroscopy could be proposed to this end.

Short and medium chains (C6, C8, and C10) allow flexibility of movement, with FA molecules managing to effectively anchor on the metal surface and promote the reaction described in Eq. 6 of the following scheme [43, 44, 80–82]. The participation of ambient water, as shown in Equation, can be justified based on ambient RH (ranging between 37 and 42% in these experiments). Nonetheless, since no infrared peaks due to hydrated

carboxylates, centered at 3300 and 1630 cm^{-1} were detected during the experiments on copper surfaces, it appears that water does not participate in the carboxylate formation (*cf.* a previous work [13], where the hydrated calcium and zinc carboxylates were formed in vitro).

$$Cu + {}^{1}/_{2}O_2 \rightarrow Cu_2O \quad (4)$$

$$Cu_2O + {}^{1}/_{2}O_2 \rightarrow 2CuO \quad (5)$$

$$2RCOOH + Cu_2O \rightarrow 2RCOOCu^{(I)} + H_2O \quad (6)$$

$$2RCOOH + CuO \rightarrow RCOO_2Cu^{(II)} + H_2O \quad (7)$$

which explains the fast formation of cuprous carboxylates (1615 cm^{-1}) on pre-corroded copper and copper alloy surfaces. Our experiments on clean/polished coupons have also shown the same infrared band initially building up as an intermediate and then being transformed into cupric carboxylates.

Acid carbonyl maxima

The actual acid carbonyl infrared maximum depends majorly on the ability for hydrogen bonding between the OH and C=O of adjacent molecules [13, 83]; the stronger the intermolecular bonding, the stronger the intermolecular attraction on both groups and the higher the downshift of their maxima, as well as the line broadening of their band shapes [84–87]. The actual carbonyl absorption along with the dimer bands are typically expected to better reflect intermolecular association and proximity. However, when the fatty acids are deposited from their solutions on a metal surface, a molecular layer at the highest proximity to the metal surface develops by orienting fatty acid molecules with their carboxylic functionalities towards the surface [88]. This is reflected in the actual carbonyl infrared maxima; proper orientation enforces an attraction between the negative edge of the carbonyl and the electropositive metal surface, and a maximum of 1715–1710 cm^{-1} is observed, downshifting well below 1700 cm^{-1}, reaching 1685 cm^{-1}. In most of our spectra, both maxima at 1710–1700 and 1690–1685 cm^{-1} are detected. This happens, presumably, due to two types of interactions, the first between the two carbonyl functionalities of paired FA molecules, typically composing a well-documented loose dimer [13, 53, 83, 89], and the second between the metal and the carbonyl functionality [90] which further downshifts the maximum at below the 1700 cm^{-1} region. This phenomenon is more obvious for the higher acids where their longer chain assists an effective orientation into self-assembled monolayers (SAM), i.e., closely packed conformations accommodating the long alkyl chains in a parallel fashion and the carboxylic groups spontaneously orienting towards the surface of metals such as gold, silver, and copper [40, 42, 88], and also, iron [39].

The reactivities of fatty acids can be explained on the above basis. The SAM phenomenon is stronger for the longer alkyl chain FA closest to the surface, as shown by the acid carbonyl infrared maxima, observed directly after deposition, which vary in the range 1710–1688 cm^{-1}. While caproic and caprylic acids (C6, and C8, respectively, Figs. 1, and 2) showed generally upshifted maxima at ~ 1710 cm^{-1}, upon consumption (and consequent thinning of the FA layer) gradually downshifted to 1705 cm^{-1} (reflecting the weak molecular organization of these acids). Capric acid (C10, Fig. 3) exhibits a 1705 cm^{-1} maximum in its thick layers (estimated at 2.9 μm, see Materials and Methods, 2.2.6), downshifting to ~ 1690 cm^{-1} when reduced to a thinner layer (< 0.4 μm). On the other hand, C14, C16, and C18 (Additional file 1: Figure S4, and Fig. 5) show an acid carbonyl doublet at ~ 1688 and 1700, reflecting an ordered assemblage of the lower FA layers, and a loose molecular organization, respectively.

Fatty diacids and protection strategies

Another interesting finding is the absence of FdiA reactivity on clean/polished pure copper and copper-zinc alloy surfaces. Suberic (C8di) and azelaic (C9di) acids showed their maxima at 1690 and 1692 cm^{-1}, respectively, both downshifted compared to their bulk values [13, 92]. This suggests the existence of closely packed organized molecular conformations on the clean (i.e., corrosion-free) copper surfaces formed by anchoring one of their two carboxylic functionalities on the metal via deprotonation and carboxylate bonding [93, 94]. These conformations can be of either (a) the self-assembled multilayer type, near-vertically tethered on the metal surface through gauche (Scheme 1d) and zigzag (Scheme 1e) conformations, previously reported to occur in the bulk [13, 77] or (b) a near-horizontal array type, stabilized on the metal surface by self-complementary, hydrogen-bonded carboxyl groups. The first suggestion may better explain the complete absence of reactivity of C9di as the proposed assemblage of Scheme 1e may account for the downshifting of the acid carbonyl band to 1694 cm^{-1} (similar to that on the gold mirror) as compared to its bulk value at 1700 cm^{-1}; besides, this arrangement may work as an effective barrier for oxygen and moisture, preventing their attack on the copper surface. Similar self-assembled structures have been previously detected in the case of aromatic diacids on copper [93]. Further evidence for the above can be provided in future research through atomic force microscopy (AFM) and scanning tunneling microscopy (STM). On the other

hand, the immediate carboxylate formation by diacids on pre-corroded surfaces suggests a fast substitution reaction between the diacids and the copper oxide(s), similar to that of fatty monoacids, that leads to the formation of carboxylates. The fact that the FdiA infrared bands remain stable within the time range of our observation at room temperature, implies that no redox reaction or other similar transformation takes place. Given the fact that a discussion has been going on regarding the anti-corrosion action on metal surfaces through the use of fatty acids [95], carboxylates and oxalates [96, 97], and SAMs [43], the use of FdiA could be added as a possible protective strategy, which opens a channel for promising future research.

Applications in archaeometry

From the standpoint of organic residues on archaeological copper surfaces [14], the detection of a 1585 cm^{-1} infrared band in a sample suggests a carboxylate that can be linked to a fatty acid precursor hydrolytically produced from a fatty ester. Besides, in the case of brass objects (i.e. Cu–Zn alloy), the presence of an additional double maximum at ~ 1550 and ~ 1525 cm^{-1} can be connected with the presence of low and medium alkyl chain (C6, C8, and C10) fatty acids, while a maximum at 1537–1540 cm^{-1}, with the presence of higher acids (C14-C18).

Besides, based on the results of this research, it could be reasonable to theorize that detection of the 1615 cm^{-1} band is an indication of the action by C10 or lower FA deposited on pre-corroded copper alloys. On the other hand, the detection of other carboxylates but the absence of this specific band could either mean FA higher than C10, or FA of the lower range deposited on non-corroded copper alloy. The entire group of both copper and zinc carboxylates, in general, could work as molecular markers providing useful information regarding the type of substances that were kept in copper containers, indirectly specifying their uses and function.

A proposed variation of copper-based dosimeters

The variable reactivity of FAs on copper surfaces may apply as a possible variation of the Oddy test [98–100]. This generally involves dosimeters made of copper or other metal foils or coupons, originally proposed and used for monitoring volatile corrosive environmental pollutants. In light of the modifications that have been proposed for adapting and developing the test [101, 102], and also taking the lead from a previous report on the formation of copper soaps on reference copper alloy plates [103], it can be proposed that if an organic solvent extract of a free FA-containing organic material or residue is dripped on copper, or brass-made dosimeters, copper or copper-zinc carboxylates (depending on the type of metal), may be formed, which can be spotted by visual inspection.

Furthermore, and more importantly, in light of the results of this work, the above application has more particularly the capability to distinguish between various FA chain lengths by simply inspecting the copper corrosion state at certain intervals, on the basis that low-mid FAs are expected to form carboxylates within hours, while the higher ones, within days. Besides, given the volatility of the lower acids, contactless formation of carboxylates may be expected, by simply exposing the dosimeter in vapor-saturated residue-containing closed spaces. This way, the presence of fatty acids in certain environments can be monitored by the use of this method and thus be a useful tool in the hands of conservators and museum caretakers.

Conclusions

All investigated fatty acids are reactive on copper and copper-zinc alloy surfaces forming the corresponding carboxylates. Their diverse reactivity depends (a) on their alkyl chain length (FA with longer alkyl chains react slower), (b) on whether they have one or two functionalities (i.e., monoacids or diacids), (c) on the elemental composition and (d) on the condition of copper surfaces. Lower and mid-chain fatty monoacids deposited on freshly cleaned/polished surfaces (i.e. carrying minimal corrosion in the form of oxides), initially form an intermediate copper carboxylate species (signature peak at 1614 cm^{-1}), which is subsequently transformed into the major Cu(II) carboxylate with a signature peak at 1585 cm^{-1}. In pre-corroded copper surfaces, the former band is immediately observed along with the other carboxylates. It could be argued that the detection of this infrared peak in archaeological organic residues may reflect the initial condition of the copper or copper alloy surface, drawing implications on the archaeometry level; however, caution is needed in the interpretation of such results as short-chain MFAs, along with the more prominent FdiAs might be the degradation routes end-products of unsaturated FAs. The detection of certain carboxylates in organic residues within archaeological copper objects can be connected to their corresponding FA precursors, i.e., short, mid, and long chains, and lead to an indirect determination of the organic substance stored in a container.

The absence of reactivity of fatty diacids on clean copper surfaces is an interesting phenomenon that could contribute to fatty acid-based strategies for the protection of copper objects. More work is needed to further investigate this phenomenon and its applications; specifically, the possible protecting action of diacids on copper surfaces could be evaluated via E_{corr} and electrochemical

impedance measurements on copper alloys at various conditions.

Finally, the relative intensities between the acid carbonyl and the various carboxylate infrared bands and the way they are connected with the reactivities of the various acids could work towards developing an extension of the Oddy test.

Abbreviations

FA	Fatty acids
FMA	Fatty monoacids
FdiA	Fatty diacids
MC	Metal carboxylates
CuC	Copper carboxylates
ZnC	Zinc carboxylates
CudiC	Copper diacid carboxylates [≠ dicarboxylates!]
ZndiC	Zinc diacid carboxylates [≠ dicarboxylates!]
SAM	Self-assembled monolayers

Supplementary Information

The online version contains supplementary material available at https://doi.org/10.1186/s40494-023-01023-1.

Additional file 1: Figure S1. FTIR spectra of authentic copper carboxylates. Infrared spectra (the 1650–1150 cm^{-1} region) of authentic copper carboxylates C6, C8, C10, C12, C14, C16, C18, C8di, and C9di. **Table S1.** Selected infrared maxima and melting points of fatty acids and the corresponding copper carboxylate authentics. **Figure S2.** C6. Indicative kinetics of the carboxylic acid C6 and C8 and the corresponding carboxylate bands: (a) caproic acid (C6), and the caproate species on Cu–Zn alloy; runs on copper metal could not be successfully followed as due to reparation the acid was elusive; caprylic acid (C8) on (b) copper and (c) copper-zinc alloy surface. Data points in (a) were obtained from original spectra, while data points in (b) and (c) were obtained from normalized spectra for compensating loss due to evaporation. **Figure S3.** FTIR of polished/clean and corroded Cu surfaces. Infrared spectra of metal surfaces (a) clean/polished Cu surface; (b) clean/polished Cu–Zn alloy surface; (c) pre-corroded Cu surface; (d) pre-corroded Cu–Zn alloy surface; and (e) for comparison, C14 immediately after deposition on clean/polished Cu–Zn alloy surface. Copper corrosion products on (c) and (d) appear as *Reststrahlen* bands at the right end of the spectra. **Figure S4**. C14. The region 1800 – 1500 cm^{-1} of consecutive spectra of C14 after deposition on clean/polished surfaces (a) copper, and (b) Cu–Zn alloy. Runs conducted at 20 °C. **Figure S5**. Consecutive spectra of C16 after deposition on Cu–Zn alloy clean/polished surfaces; (a) full spectra; (b) zoom in the region 1800 – 1500 cm^{-1}. Runs conducted at 40 °C. **Figure S6.** Indicative kinetics of C18 showing acidic carbonyl (1699 cm^{-1}) and carboxylate (1585 cm^{-1}). **Figure S5**. Corresponding absorbance time drives of C18 carboxylic acid and carboxylate bands on (a) pure Cu, and (b) Cu–Zn alloy surface. **Table S2.** Estimation of fatty acid film thicknesses on metal surfaces.

Acknowledgements
The authors wish to thank Prof. George Mastrotheodoros (University of West Attica) for assisting with XRF measurements.

Author contributions
SB: conceptualization, research design, and planning, infrared spectroscopy, manuscript writing, and revision. LF-L: infrared spectroscopy, melting points recording, thermal behavior of authentic metal copper salts, partial manuscript writing. MG: conceptualization of the copper-fatty acid interface, and applications. AF: synthesis of the fatty copper salts authentics.

Funding
This work has been orally presented at Chemistry for Cultural Heritage (ChemCH2020) Congress in Ravenna, 4–8 July 2022, where participation of corresponding author was funded by the Special Account of Research Funds of the University of West Attica. It was also, in part enabled by the University of West Attica adjunct professorship funding for the participation of Dr. Leonidas Fragkos-Livanios.

Availability of data and materials
The authors declare that the data supporting the findings of this study are available within the paper and its Supplementary Information files. Should any raw data files be needed in another format they are available from the corresponding author upon reasonable request. Source data are provided with this paper.

Declarations

Competing interests
The authors have no competing interests as defined by Springer, or other interests that might be perceived to influence the results and/or discussion reported in this paper. No competing are declared by the authors. No testing on animals was conducted.

Received: 29 March 2023 Accepted: 8 August 2023

References

1. Mills JS. The organic chemistry of museum objects. 2nd ed. Oxford, UK: Butterworth-Heinemann; 2003.
2. Mills JS. The gas chromatographic examination of paint media. Part I. Fatty acid composition and identification of dried oil films. Stud Conserv. 1966;11:92–107.
3. mills JS, white r. the Gas-Chromatographic Examination of Paint Media. Part II. Some examples of medium identification in paintings by fatty acid analysis. Stud Conserv. 1972;17:721–8.
4. Nawar WW. Thermal degradation of lipids. J Agric Food Chem. 1969;17:18–21.
5. Pellegrini D, Duce C, Bonaduce I, et al. Fourier transform infrared spectroscopic study of rabbit glue/inorganic pigments mixtures in fresh and aged reference paint reconstructions. Microchem J. 2016;124:31–5.
6. Degano I, La Nasa J, Ghelardi E, et al. Model study of modern oil-based paint media by triacylglycerol profiling in positive and negative ionization modes. Talanta. 2016;161:62–70.
7. Garnier N, Rolando C, Høtje JM, Tokarski C. Analysis of archaeological triacylglycerols by high resolution nanoESI, FT-ICR MS and IRMPD MS/MS: application to 5th century BC–4th century AD oil lamps from Olbia (Ukraine). Int J Mass Spectrom. 2009;284:47–56.
8. Gregg MW, Slater GF. A new method for extraction, isolation and transesterification of free fatty acids from archaeological pottery. Archaeometry. 2010;52:833–54.
9. Regert M, Garnier N, Decavallas O, et al. Structural characterization of lipid constituents from natural substances preserved in archaeological environments. Meas Sci Technol. 2003;14:1620–30.
10. Modugno F, Di Gianvincenzo F, Degano I, et al. On the influence of relative humidity on the oxidation and hydrolysis of fresh and aged oil paints. Sci Rep. 2019;9:1–16.
11. Banti D, La Nasa J, Tenorio AL, et al. A molecular study of modern oil paintings: Investigating the role of dicarboxylic acids in the water sensitivity of modern oil paints. RSC Adv. 2018. https://doi.org/10.1039/c7ra13364b.
12. Bonaduce I, Carlyle L, Colombini MP, et al. New insights into the ageing of linseed oil paint binder: a qualitative and quantitative analytical study. PLoS ONE. 2012;7:e49333.
13. Filopoulou A, Vlachou S, Boyatzis SC. Fatty acids and their metal salts: a review of their infrared spectra in light of their presence in cultural heritage. Molecules. 2021;26:6005.
14. Koupadi K, Boyatzis SC, Roumpou M, et al. Organic remains in early Christian Egyptian metal vessels: investigation with fourier transform infrared spectroscopy and gas chromatography-mass spectrometry. Heritage. 2021;4:3611–29.

15. Craig OE, Saul H, Spiteri C. Residue analysis. In: Richards M, Britton K, editors. Archaeological science. Cambridge, UK: Cambridge University Press; 2019. p. 70–98.
16. Evershed RP, Berstan R, Grew F, et al. Formulation of a Roman cosmetic. Nature. 2004;432:35–6.
17. Frith J, Appleby R, Stacey R, Heron C. Sweetness and light: chemical evidence of beeswax and tallow candles at fountains Abbey, North Yorkshire. Mediev Archaeol. 2004;48:220–7.
18. Ribechini E, Modugno F, Baraldi C, et al. An integrated analytical approach for characterizing an organic residue from an archaeological glass bottle recovered in Pompeii (Naples, Italy). Talanta. 2008;74:555–61.
19. Schrenk J. Royal Benin Art: Surfaces, Past and Present. In: David A. Scott, Podany J, Considine BB (eds) Proceedings of the International Symposium of Ancient and Historic Metals: Conservation and Scientific Research. The J. Paul Getty Museum and The Getty Conservation Institute, Los Angeles. 1994; pp 51–62
20. Pavlopoulou L (2017) Chemical, Physical and Mechanical Decay Procedures in Oil painted Copper Objects. In: Fuster López L (ed) Paintings on Copper (and other metal plates). Production, degradation and conservation issues, Universitat Politècnica de Valencia. 2017:27-28. Universitat Politècnica de Valencia, Valencia
21. Pavlopoulou L-C, Watkinson D. The degradation of oil painted copper surfaces. Stud Conserv. 2006;51:55–65.
22. Boon JJ, Hoogland F, Keune K, Parkin HM. Chemical processes in aged oil paints affecting metal soap migration and aggregation. Provid Rhode Island: AIC Paint Spec Gr Postprints; 2006. p. 16–23.
23. Hermans JJ. Metal soaps in oil paint: Structure, mechanisms and dynamics. University of Amsterdam; 2017.
24. Hermans JJ, Keune K, Van Loon A, Iedema PD. Toward a complete molecular model for the formation of metal soaps in oil paints. In: Casadio F, Keune K, Noble P, Loon A, Hendriks E, Centeno SA, Osmond G, editors. Metal soaps in art. Cham: Springer; 2019. p. 47–67.
25. Hermans JJ, Keune K, Van Loon A, Iedema PD. The crystallization of metal soaps and fatty acids in oil paint model systems. Phys Chem Chem Phys. 2016;18:10896–905.
26. Hermans J, Helwig K. The identification of multiple crystalline Zinc soap structures using infrared spectroscopy. Supplemental information. Appl Spectrosc. 2020;74:1505–14.
27. Cotte M, Checroun E, De Nolf W, et al. Lead soaps in paintings: friends or foes? Stud Conserv. 2017. https://doi.org/10.1080/00393630.2016.1232529.
28. Scott DA, Taniguchi Y, Koseto E. The verisimilitude of verdigris: a review of the copper carboxylates. Stud Conserv. 2001;46:73–91.
29. Melo MJ, Castro R (2020) Making verdigris (from copper). In: Melo MJ, Castro R (eds) The "book on how to make colours." Universidade Nova de Lisboa, School of Science and Technology, Departamento de Conservacao e Restauro, Lisbon
30. Chaplin TD, Clark RJH, Scott DA. Study by Raman microscopy of nine variants of the green-blue pigment verdigris. J Raman Spectrosc. 2006;37:223–9.
31. Bette S, Eggert G, Dinnebier RE. Crystalline materials in art and conservation: verdigris pigments—what we know and what we still don't know. Phys Sci Rev. 2023. https://doi.org/10.1515/psr-2018-0154.
32. Brostoff LB, Connelly Ryan C. Tracing the alteration of verdigris pigment through combined Raman spectroscopy and x-ray diffraction, part i. Restaurator. 2020;41:3–30.
33. Dobry A, Mahncke HE. Reaction of stearic acid monolayers with copper and cuprous oxide. Nature. 1954;174:507.
34. Ross RA, Takacs A. Heterogeneous reactions of aluminum and copper surfaces with stearic acid. Ind Eng Chem Prod Res Dev. 1983;22:280–6.
35. Tilbrooke D. The fatty acid corrosion of copper alloys and its treament. ICCM Bull. 1980;6:46–52.
36. Daniels V. Analyses of copper- and beeswax-containing green paint on Egyptian antiquities. Stud Conserv. 2007;52:13–8.
37. Gramtorp D, Botfeldt K, Glastrup J, Simonsen KP. Investigation and conservation of Anne Marie Carl-Nielsen's wax models. Stud Conserv. 2015;60:97–106.
38. Brühl B. Copper Soaps on Ethnographic and Decorative Art Objects. In: Hyslop E, Gonzalez V, Troalen L, Wilson L (eds) Metal 2013, 16th-20th September 2013: Interim meeting of the ICOM-CC Metal Working Group. Edinburgh, Scotland. 2013; pp 265–269
39. Loehle S. Understanding of adsorption mechanisms and tribological behaviors of C18 fatty acids on iron-based surfaces: a molecular simulation approach. University of Lyon; 2014.
40. Whelan CM, Ghijsen J, Pireaux JJ, Maex K. Cu adsorption on carboxylic acid-terminated self-assembled monolayers: a high-resolution X-ray photoelectron spectroscopy study. Thin Solid Films. 2004;464–465:388–92.
41. Buckholtz GA, Gawalt ES. Effect of alkyl chain length on carboxylic acid SAMs on Ti-6Al-4V. Materials (Basel). 2012;5:1206–18.
42. Jadhav SA. Self-assembled monolayers (SAMs) of carboxylic acids: An overview. Cent Eur J Chem. 2011;9:369–78.
43. Telegdi J. Formation of self-assembled anticorrosion films on different metals. Materials (Basel). 2020;13:1–25.
44. da Carvalho LC. Beyond copper soaps. Characterization of copper corrosion containing organics. Cham: Springer International Publishing; 2022.
45. Beerse M, Keune K, Iedema P, et al. Evolution of zinc carboxylate species in oil paint ionomers. ACS Appl Polym Mater. 2020;2:5674–85.
46. Robinet L, Corbeil MC. The characterization of metal soaps. Stud Conserv. 2003;48:23–40.
47. Otero V, Sanches D, Montagner C, et al. Characterisation of metal carboxylates by Raman and infrared spectroscopy in works of art. J Raman Spectrosc. 2014;45:1197–206.
48. Hermans JJ, Keune K, Van Loon A, et al. Ionomer-like structure in mature oil paint binding media. RSC Adv. 2016. https://doi.org/10.1039/c6ra18267d.
49. Hermans JJ, Baij L, Koenis M, et al. 2D-IR spectroscopy for oil paint conservation: elucidating the water-sensitive structure of zinc carboxylate clusters in ionomers. Sci Adv. 2019;5:1–10.
50. Deacon GB, Phillips RJ. Relationships between the carbon-oxygen stretching frequencies of carboxylato complexes and the type of carboxylate coordination. Coord Chem Rev. 1980;33:227–50.
51. Crowell JE, Chen JG, Yates JT. A vibrational study of the adsorption and decomposition of formic acid and surface formate on Al(111). J Chem Phys. 1986;85:3111–22.
52. Nakamoto K. Infrared and Raman spectra of Inorganic and Coordination Compounds, Part B, applications in coordination, organometallic, and bioinorganic chemistry. 6th ed. Hoboken, New Jersey: John Wiley & Sons; 2009.
53. Boyatzis SC. Materials in art and archaeology through their infrared spectra. New York: Nova Science Publishers; 2022.
54. Strommen DP, Giroud-Godquin AM, Maldivi P, et al. Vibrational studies of some dicopper tetracarboxylates which exhibit a thermotropic columnar mesophase. Liq Cryst. 1987;2:689–99.
55. Nordin N, Samad ZW, Yusop RM, Othman MR. Synthesis and characterization of copper(II) carboxylate with palm-based oleic acid by electrochemical technique. Artic Malaysian J Anal Sci. 2015;19:236–43.
56. Hermans J, Zuidgeest L, Iedema P, et al. The kinetics of metal soap crystallization in oil polymers. Phys Chem Chem Phys. 2021;23:22589–600.
57. Corbeil M-C, Robinet L. X-ray powder diffraction data for selected metal soaps. Powder Diffr. 2002;17:52–60.
58. Thickett D, Pretzel B. FTIR surface analysis for conservation. Herit Sci. 2020;8:1–10.
59. Finke SJ, Schrader GL. Infrared reflection-absorption spectroscope using thin film structures. Spectrochim Acta Part A Mol Spectrosc. 1990;46:91–6.
60. Golden WG, Dunn DS, Overend J. A method for measuring infrared reflection-absorption spectra of molecules adsorbed on low-area surfaces at monolayer and submonolayer concentrations. J Catal. 1981;71:395–404.
61. Boyatzis S, Douvas AM, Argyropoulos V, et al. Characterization of a water-dispersible metal protective coating with fourier transform infrared spectroscopy, modulated differential scanning calorimetry, and ellipsometry. Appl Spectrosc. 2012;66:580–90.
62. Hosoi Y, Niwa Y, Sakurai Y, et al. IRRAS and LEED studies of films of the long chain n-alkane n-C44H90 on Cu(1 0 0) and Cu(1 1 0). Appl Surf Sci. 2003;212–213:441–5.

63. Smith DM, Chughtai AR. Polymer optical and dielectric properties through vibrational spectroscopy. In: Everall NJ, editor. Handbook of vibrational spectroscopy. Chichester, UK: John Wiley & Sons Ltd; 2007.
64. Griffiths PR, de Haseth JA. Fourier transform infrared spectrometry. 2nd ed. Hoboken, New Jersey: John Wiley & Sons Inc; 2007.
65. Merklin GT. Infrared spectrometry of thick organic films on metallic substrates. In: Griffiths PR, editor. Handbook of vibrational spectroscopy. Chichester, UK: John Wiley & Sons Ltd; 2006.
66. Sinclair RG, McKay AF, Jones RN. The infrared absorption spectra of saturated fatty acids and esters. J Am Chem Soc. 1952;74:2570–5.
67. Norman Jones R, McKay AF, Sinclair RG. Band progressions in the infrared spectra of fatty acids and related compounds. J Am Chem Soc. 1952;74:2575–8.
68. Meiklejohn RA, Meyer RJ, Aronovic SM, et al. Characterization of long-chain fatty acids by infrared spectroscopy. Anal Chem. 1957;29:329–34.
69. Chapman D. Infrared spectroscopy of lipids. J Am Oil Chem Soc. 1965;42:353–71.
70. Kenar JA, Moser BR, List GR. Naturally occurring fatty acids source, chemistry, and uses. In: Ahmad MU, editor. Fatty acids. Chemistry, synthesis, and applications. London: Academic Press and AOCS Press; 2017. p. 23–82.
71. Lee J, Bonaduce I, Modugno F, et al. Scientific investigation into the water sensitivity of twentieth century oil paints. Microchem J. 2018;138:282–95.
72. Colombini MP, Modugno F, Giacomelli M, Francesconi S. Characterisation of proteinaceous binders and drying oils in wall painting samples by gas chromatography-mass spectrometry. J Chromatogr A. 1999;846:113–24.
73. Hermans JJ, Keune K, Van Loon A, Iedema PD. An infrared spectroscopic study of the nature of zinc carboxylates in oil paintings. J Anal At Spectrom. 2015;30:1600–8.
74. Wojciechowski K, Bitner A, Bernardinelli G, Brynda M. Azacrown ether-copper(II)-hexanoate complexes. from monomer to 1-D metal organic polymer. Dalt Trans. 2009;7:1114–22.
75. Fawcett WR. Chemical reaction kinetics in solution. In: Fawcett WR, editor. Liquids, solutions, and interfaces. Oxford: Oxford University Press; 2004.
76. Kamm GE, Huang G, Vornholt SM, et al. Relative kinetics of solid-state reactions: the role of architecture in controlling reactivity. J Am Chem Soc. 2022;144:11975–9.
77. Thalladi VR, Nüsse M, Boese R. The melting point alternation in α, ω-alkanedicarboxylic acids. J Am Chem Soc. 2000;122:9227–36.
78. Kanicky JR, Shah DO. Effect of degree, type, and position of unsaturation on the pKa of long-chain fatty acids. J Colloid Interface Sci. 2002;207:201–7.
79. Pashkovskaya AA, Vazdar M, Zimmermann L, et al. Mechanism of long-chain free fatty acid protonation at the membrane-water interface. Biophys J. 2018;114:2142–51.
80. MacLeod ID. Bronze disease: an electrochemical explanation. ICCM Bull. 1981;7:16–26.
81. Qiu P, Leygraf C. Initial oxidation of brass induced by humidified air. Appl Surf Sci. 2011;258:1235–41.
82. Leygraf C, Wallinder IO, Tidblad J, Graedel T. Atmospheric corrosion. 2nd ed. Hoboken, NJ: Wiley; 2016.
83. Mayo D, Miller F, Hannah R. Course notes on the interpretation of infrared and Raman spectra. Hoboken, NJ, USA: John Wiley & Sons Inc; 2004.
84. Kaneko F, Tashiro K, Kobayashi M. Polymorphic transformations during crystallization processes of fatty acids studied with FT-IR spectroscopy. J Cryst Growth. 1999;198–199:1352–9.
85. Conti G, Minoni G, Zerbi G. E → C phase transition in fatty acids: a spectroscopic study. J Mol Struct. 1984;118:237–43.
86. Zerbi G, Conti G, Minoni G, et al. Premelting phenomena in fatty acids: an infrared and Raman study. J Phys Chem. 1987;91:2386–93.
87. Bezrodna T. Temperature dynamics of dimer formation in behenic acid: FT-IR spectroscopic study. J Mol Struct. 2013;1040:112–6.
88. Pawsey S, Yach K, Halla J, Reven L. Self-assembled monolayers of alkanoic acids: a solid-state NMR study. Langmuir. 2000;16:3294–303.
89. Coates J. Interpretation of infrared spectra, a practical approach. In: encyclopedia of analytical chemistry. Chichester, UK: John Wiley & Sons, Ltd.; 2006. p. 10815–37.
90. Lu Y, Miller JD. Carboxyl stretching vibrations of spontaneously adsorbed and LB-transferred calcium carboxylates as determined by FTIR internal reflection spectroscopy. J Colloid Interface Sci. 2002;256:41–52.
91. Tafipolsky M, Schmid R. A consistent force field for the carboxylate group. J Chem Theory Comput. 2009;5:2822–34.
92. Banou P, Boyatzis S, Choulis K, et al. Oil media on paper: investigating the effect of linseed oils on lignocellulosic paper supports. Analytica. 2022;3:266–86.
93. Schmitt T, Hammer L, Schneider MA. Evidence for on-site carboxylation in the self-assembly of 4,4′-Biphenyl Dicarboxylic acid on Cu(111). J Phys Chem C. 2016;120:1043–8.
94. Aitchison H, Lu H, Hogan SWL, et al. Self-assembled monolayers of oligophenylenecarboxylic acids on silver formed at the liquid-solid interface. Langmuir. 2016;32:9397–409.
95. Elia A, Dowsett M, Adriaens A. On the use of alcoholic carboxylic acid solutions for the deposition of protective coatings on copper. In: Mardikian P, Chemello C, Watters C, Hull P (eds) International Conference of Metal Conservation Interim Meeting of the International Council of Museums Committee for Conservation Metal Working Group ICOM 2010. Clemson University, Charleston. 2010; pp 144–150
96. Hollner S, Mirambet F, Texier A, et al. Development of new non-toxic inhibitors for cultural propert made of iron and copper alloys. In: Argyropoulos V, Hein A, Harith MA (eds) Strategies for Saving our Cultural Heritage, Conference Proceeding held in Cairo, Egypt, 25 February – 1 March 2007. TEI of Athens, Cairo. 2007; p 156
97. Otero V, Vilarigues M, Carlyle L, et al. A: Little key to oxalate formation in oil paints: protective patina or chemical reactor? Photochem Photobiol Sci. 2018;17:266–70.
98. Oddy WA. Chemistry in the conservation of archaeological materials. Sci Total Environ. 1994;143:121–6.
99. Oddy T, Museum B, Oddy A. Oddy test. 2003; 1–7
100. Bamberger JA, Howe EG, Wheeler G. A variant Oddy test procedure for evaluating materials used in storage and display cases. Stud Conserv. 1999;44:86–90.
101. Díaz I, Cano E. Quantitative Oddy test by the incorporation of the methodology of the ISO 11844 standard: a proof of concept. J Cult Herit. 2022;57:97–106.
102. Korenberg C, Keable M, Phippard J, Doyle A. Refinements introduced in the Oddy test methodology. Stud Conserv. 2018;63:2–12.
103. Brühl B (2012) Copper Soaps on Ethnographic and Decorative Art Objects. In: The Decorative. Conservation Applied Arts, IIC Congress. Vienna, p 1

Publisher's Note